Informes Técnicos Ciemat

1378

Diciembre, 2015

# Gas Transport in Opalinus Clay

M. V. Villar
F. J. Romero
P. L. Martín
V. Gutiérrez-Rodrigo
J. M. Barcala

GOBIERNO DE ESPAÑA

MINISTERIO DE ECONOMÍA Y COMPETITIVIDAD

Ciemat
Centro de Investigaciones Energéticas, Medioambientales y Tecnológicas

Informes Técnicos Ciemat

**1378**

Diciembre, 2015

# Gas Transport in Opalinus Clay

M. V. Villar
F. J. Romero
P. L. Martín
V. Gutiérrez-Rodrigo
J. M. Barcala

**Departamento de Medio Ambiente**

Toda correspondencia en relación con este trabajo debe dirigirse al Servicio de Información y Documentación, Centro de Investigaciones Energéticas, Medioambientales y Tecnológicas, Ciudad Universitaria, 28040-MADRID, ESPAÑA.

Las solicitudes de ejemplares deben dirigirse a este mismo Servicio.

Los descriptores se han seleccionado del Thesauro del DOE para describir las materias que contiene este informe con vistas a su recuperación. La catalogación se ha hecho utilizando el documento DOE/TIC-4602 (Rev. 1) Descriptive Cataloguing On-Line, y la clasificación de acuerdo con el documento DOE/TIC.4584-R7 Subject Categories and Scope publicados por el Office of Scientific and Technical Information del Departamento de Energía de los Estados Unidos.



Catálogo general de publicaciones oficiales
http://www.060.es

**Depósito Legal**: M-26385-2011
**ISSN:** 1135-9420
**NIPO:** 721-15-075-9

Editorial CIEMAT

CLASIFICACIÓN DOE Y DESCRIPTORES

S58
STRATIFICATION; GASES; PERMEABILIY; OPALINUS CLAY; UNDERGROUND DISPOSAL; GEOLOGIC SURVEYS

# Gas Transport in Opalinus Clay

Villar, M. V.; Romero, F. J.; Martín, P.L.; Gutiérrez-Rodrigo, V.; Barcala, J. M.
48 pp. 6 ref. 48 figs. 5 tables

**Abstract:**

An experimental setup was designed to measure gas permeability and gas breakthrough pressures. It was able to apply gas injection pressures of up to 18 MPa to cylindrical samples submitted to higher confining pressures while measuring the gas otflow. Nine gas permeability tests were performed in triaxial cells with Opalinus clay samples of the shaly facies obtained by drilling from the BDR-1 core in the sense perpendicular to bedding. The average dry density of the samples was 2.31±0.04 g/cm$^3$ and water content of 4.5±1.8% ($S_r$=69±22%). The samples were not saturated prior or during the gas testing. The confining pressures applied in these tests were higher than the maximum in situ stress, and the tests were performed by slowly increasing the injection pressure whereas backpressure was kept atmospheric and the outflow was measured. These tests showed that the breakthrough pressure in the sense perpendicular to bedding was generally higher than 18 MPa (effective pressure of 11.5 MPa), although in a few instances flow occurred for lower pressures. When this happened, the gas permeability measured ($k_{ig}{\cdot}k_{rg}$) was in the range from $8{\cdot}10^{-21}$ to $4{\cdot}10^{-23}$ m$^2$ (average $k_g$ of $1.8{\cdot}10^{-15}$ m/s), decreasing very slightly with confining pressure. The air entry value deduced from mercury intrusion porosimetry tests for this material was between 19 and 36 MPa.

The hydraulic conductivity in the sense normal to bedding obtained under effective stress conditions of 0.8 MPa (void ratio 0.24) was $2.7{\cdot}10^{-14}$ m/s (corresponding to an intrinsic permeability of $2.7{\cdot}10^{-21}$ m$^2$).

# Transporte de Gas en la Arcilla Opalinus

Villar, M. V.; Romero, F. J.; Martín, P.L.; Gutiérrez-Rodrigo, V.; Barcala, J. M.
48 pp. 6 ref. 48 figs. 5 tables

**Resumen:**

Se ha diseñado un dispositivo experimental para medir permeabilidad al gas y presión de paso de aire, capaz de aplicar presiones de inyección de hasta 18 MPa a muestras cilíndricas sometidas a presiones confinantes mayores y de medir simultáneamente el flujo de salida. En este informe se recogen los resultados de nueve ensayos realizados en muestras de la facies arcillosa de la arcilla Opalinus de densidad seca 2,31±0,04 g/cm$^3$ y humedad 4,5±1,8% ($S_r$=69±22%) perforadas en el testigo BDR-1 en sentido perpendicular a la estratificación,. No se saturaron las muestras ni antes ni durante los ensayos. Se aplicaron presiones confinantes mayores que la tensión máxima in situ, y los ensayos consistieron en aumentar lentamente la presión de inyección mientras la presión de cola se mantenía atmosférica y se medía el flujo de gas de salida. Los ensayos mostraron que la presión de paso de aire en sentido perpendicular a la estratificación es generalmente mayor de 18 MPa (presión efectiva de 11,5 MPa), aunque en unos pocos casos sí se produjo flujo para presiones menores. En esos casos, la permeabilidad al gas medida ($k_{ig}{\cdot}k_{rg}$) fue de $8{\cdot}10^{-21}$ a $4{\cdot}10^{-23}$ m$^2$ ($k_g$ media de $1.8{\cdot}10^{-15}$ m/s), con una ligera tendencia a disminuir con la presión confinante. La presión de entrada de aire para este material deducida de los ensayos de porosimetría por intrusión de mercurio está entre 19 y 36 MPa.
La conductividad hidráulica en sentido perpendicular a la estratificación obtenida bajo una tensión efectiva de 0,8 MPa (índice de poros de 0,24) es de $2,7{\cdot}10^{-14}$ m/s (correspondiente a una permeabilidad intrínseca de $2,7{\cdot}10^{-21}$ m$^2$).

# Gas transport in Opalinus clay

Technical Report CIEMAT/DMA/2G207/1/15

M.V. Villar, F.J. Romero, P.L. Martín,
V. Gutiérrez-Rodrigo, J.M. Barcala

FORGE
Fate Of Repository Gases
European Commission FP7

EURATOM

# Summary

An experimental setup was designed to measure gas permeability and gas breakthrough pressures. It was able to apply gas injection pressures of up to 18 MPa to cylindrical samples submitted to higher confining pressures while measuring the gas otflow. Nine gas permeability tests were performed in triaxial cells with Opalinus clay samples of the shaly facies obtained by drilling from the BDR-1 core in the sense perpendicular to bedding. The average dry density of the samples was 2.31±0.04 g/cm$^3$ and water content of 4.5±1.8% ($S_r$=69±22%). The samples were not saturated prior or during the gas testing. The confining pressures applied in these tests were higher than the maximum *in situ* stress, and the tests were performed by slowly increasing the injection pressure whereas backpressure was kept atmospheric and the outflow was measured. These tests showed that the breakthrough pressure in the sense perpendicular to bedding was generally higher than 18 MPa (effective pressure of 11.5 MPa), although in a few instances flow occurred for lower pressures. When this happened, the gas permeability measured ($k_{ig}$·$k_{rg}$) was in the range from 8·10$^{-21}$ to 4·10$^{-23}$ m$^2$ (average $k_g$ of 1.8·10$^{-15}$ m/s), decreasing very slightly with confining pressure. The air entry value deduced from mercury intrusion porosimetry tests for this material was between 19 and 36 MPa.

The hydraulic conductivity in the sense normal to bedding obtained under effective stress conditions of 0.8 MPa (void ratio 0.24) was 2.7·10$^{-14}$ m/s (corresponding to an intrinsic permeability of 2.7·10$^{-21}$ m$^2$).

# Resumen

Se ha diseñado un dispositivo experimental para medir permeabilidad al gas y presión de paso de aire, capaz de aplicar presiones de inyección de hasta 18 MPa a muestras cilíndricas sometidas a presiones confinantes mayores y de medir simultáneamente el flujo de salida. En este informe se recogen los resultados de nueve ensayos realizados en muestras de la facies arcillosa de la arcilla Opalinus de densidad seca 2,31±0,04 g/cm$^3$ y humedad 4,5±1,8% ($S_r$=69±22%) perforadas en el testigo BDR-1 en sentido perpendicular a la estratificación,. No se saturaron las muestras ni antes ni durante los ensayos. Se aplicaron presiones confinantes mayores que la tensión máxima in situ, y los ensayos consistieron en aumentar lentamente la presión de inyección mientras la presión de cola se mantenía atmosférica y se medía el flujo de gas de salida. Los ensayos mostraron que la presión de paso de aire en sentido perpendicular a la estratificación es generalmente mayor de 18 MPa (presión efectiva de 11,5 MPa), aunque en unos pocos casos sí se produjo flujo para presiones menores. En esos casos, la permeabilidad al gas medida ($k_{ig}$·$k_{rg}$) fue de 8·10$^{-21}$ a 4·10$^{-23}$ m$^2$ ($k_g$ media de 1.8·10$^{-15}$ m/s), con una ligera tendencia a disminuir con la presión confinante. La presión de entrada de aire para este material deducida de los ensayos de porosimetría por intrusión de mercurio está entre 19 y 36 MPa.

La conductividad hidráulica en sentido perpendicular a la estratificación obtenida bajo una tensión efectiva de 0,8 MPa (índice de poros de 0,24) es de 2,7·10$^{-14}$ m/s (correspondiente a una permeabilidad intrínseca de 2,7·10$^{-21}$ m$^2$).

# Contents

# 1 Introduction

The multiple-barrier concept is the cornerstone of all proposed schemes for underground disposal of radioactive wastes. The concept invokes a series of barriers, both engineered and natural, between the waste and the surface. Achieving this concept is the primary objective of all disposal programmes, from site appraisal and characterisation to repository design and construction. However, the performance of the repository as a whole (waste, buffer, engineering disturbed zone, host rock), and in particular its gas transport properties, are still poorly understood. Issues still to be adequately examined that relate to understanding basic processes include: dilational versus visco-capillary flow mechanisms; long-term integrity of seals, in particular gas flow along contacts; role of the EDZ as a conduit for preferential flow; laboratory to field up-scaling. Of particular importance are the long-term performance of bentonite buffers, plastic clays, indurated mudrocks and crystalline formations. Further experimental data are required to reduce uncertainty relating to the quantitative treatment of gas in performance assessment. Understanding gas generation and migration is thus vital in the quantitative assessment of repositories and was the focus of the research in the integrated, multi-disciplinary project FORGE. The FORGE project was a pan-European project with links to international radioactive waste management organisations, regulators and academia, specifically designed to tackle the key research issues associated with the generation and movement of repository gasses. FORGE addressed these issues through a series of laboratory and field-scale experiments, including the development of new methods for up-scaling allowing the optimisation of concepts through detailed scenario analysis. Further details on the FORGE project and its outcomes can be accessed at www.FORGEproject.org.

This report includes part of the work carried out by CIEMAT in FORGE WP5.1 “Gas transport laboratory experiments”, which included two kinds of tests in indurated clay (the Opalinus clay): the determination of 2-phase flow parameters (Villar & Romero 2012) and gas permeability and gas breakthrough pressure determinations, which are the topic of this report.

For the determination of the gas permeability and gas breakthrough pressure a setup was designed and fine-tuned. It allowed the application of gas injection pressures of up to 18 MPa to cylindrical samples while keeping higher confining pressures and measuring the gas outflow. The measurements of the stress state at Mont Terri indicate that $\sigma_1$ is 6-7 MPa (Corkum & Martin 2007), what means that the confining pressures applied in the laboratory tests have been higher than this value.

# 2 Material

The material used in the tests came from a borehole drilled in the Opalinus Clay Mesozoic formation at the Mont Terri Underground Research Laboratory (URL) in the Folded Jura mountains (http://www.mont-terri.ch). This formation is a mainly marly claystone with differing proportions of sand and carbonates around 180 million years old (Aalenian). At the URL, the Opalinus Clay has a layer thickness of around 140 m.

From a mineralogical point of view the Opalinus Clay consists of 40-80% clay minerals (including mixed layers of illite and swelling smectite), 10-40% quartz, 5-40% calcite and smaller proportions of siderite, pyrite and organic carbon. The dry density range is between 2.20 and 2.41 g/cm$^3$, the water content between 5.0 and 8.9% and the hydraulic conductivity between $2\cdot10^{-14}$ and $1\cdot10^{-12}$ m/s (Marschall et al. 2004).

Of the three facies of Opalinus Clay that can be distinguished, the materials used in this investigation belong to the shaly one, which is a homogeneous, barely visible laminated claystone with low sand content. For the gas permeability and breakthrough pressure tests a core from borehole BDR-1 was used. The total suction of this core was measured at laboratory temperature (21°C) with two capacitive sensors inserted in a suitable perforated hole (Figure 1). The equilibrium value was found to be 31.3±0.1 MPa for a dry density of 2.33 g/cm$^3$ and water content of 6.4% (determined in samples drilled from the core). The measured grain density for this sample was 2.71 g/cm$^3$.

**Figure 1: Measurement of relative humidity inside the BDR-1 core**

The water retention curves of samples from cores BHT-1 and BHG-D1 drilled also in the shaly facies of the Opalinus clay were determined under different conditions (Villar & Romero 2012). Through the fitting of these results to the van Genuchten expression, it was possible to compute the capillary strength parameter $P_0$, which was sometimes interpreted as representing the capillary pressure at which a continuous gas path is established and is frequently assimilated to the air entry value, i.e. the suction above which air is able to enter the pores of the sample, and consequently, above which 2-phase flow can take place in the soil pore structure. The $P_0$ values obtained were between 6 and 34 MPa, and tended to be higher for the samples tested under stress, in drying paths and when total suction was used. A $P_0$ value of 18 MPa was found by Romero et al. (2012) in samples of the Opalinu shaly facies taken from the BHA-8/1 core.

Additionally, a sample from the BHG-D1 core used for the determination of the water retention curves was lyophilised and analysed by mercury intrusion porosimetry (MIP). The dry density was 2.4 g/cm$^3$ and the water content 3.4% (slightly air-dried). Most of the pore sizes were comprised in the range 2-50 nm, *i.e*. in the mesopore range, with a dominant pore mode of 11 nm. The air entry value corresponding to this dominant pore mode calculated from the Laplace's equation is 27.8 MPa. Romero et al. (2012) reported an air entry value of 13 MPa in Opalinus clay samples from core BHA-8/1.

# 3 Methodology

## 3.1 EQUIPMENT

A setup was designed to perform steady gas permeability measurements under different gas pressures. The cylindrical sample was confined in a stainless steel triaxial cell that was filled with water and pressurised to the desired confining pressure. The gas injection pressure could be independently varied and kept constant during the period of time necessary to get steady gas flow, while the gas backpressure was kept atmospheric and the outflow measured.

Two different pressure lines were used to apply the confining pressure: a low-pressure line (Figure 2), in which the confining pressure was applied with a GDS pressure/volume piston controller with a working capacity of up to 16 MPa; and a high-pressure line to apply confining pressures of up to 33 MPa (Figure 3). In the latter, the water in the cell was pressurised using the gas in a pressure bladder accumulator, which took the gas from a high-pressure deposit in which nitrogen was previously compressed by a gas-booster. The gas-booster took the nitrogen from a gas cylinder and the high-pressure deposit was equipped with a high-performance high-pressure unit (valve and controller) that controlled the actual pressure value applied to the accumulator. This high-pressure deposit supplied also the nitrogen gas to a 300-$cm^3$ pressurised deposit (gas buffer) equipped with a pressure transmitter from which nitrogen was injected on top of the sample. Injection pressures of up to 18 MPa could be applied. The outlet of the cell connected to the bottom of the sample was open to atmosphere, with a series of different range gas mass flowmeters measuring the gas outflow. Outflow gas rates, up and downstream pressure, confining pressure and temperature were monitored online.

A more detailed description of the components of the experimental setup includes:

- *Test cells*. They were made of stainless steel, able of withstanding pressures up to 21 MPa (Figure 4, Figure 5). Each cell had three inlets drilled: one for sample top drainage, one for sample bottom drainage, and another one for confining pressure. Three no-volume-change valves were connected to the ports. The tests were not performed under real triaxial conditions though.
- *Gas booster*. To obtain the high gas pressures needed for the confining and injection pressures, nitrogen taken from a gas cylinder was compressed by a POWER-STAR gas-booster (up to 35 MPa, dual stage, air-operated) in a high-pressure (34.5 MPa) cylinder (Figure 6). The final pressure applied to the system was controlled by a high-performance high-pressure unit (valve and controller).
- *Gas buffer*. The gas was injected on top of the samples from a WHITEY gas sampling cylinder (DOT-3E 1800, 316L-HDF4-300, 300 $cm^3$) acting as a gas buffer to prevent fluctuations in the injection pressure. It also allowed to keep constant the expected flow even in case of pneumatic fracturing. The deposit was pressurised with the setup described above and was equipped with a pressure transmitter. Injection pressures of up to 12.4 MPa could be applied.

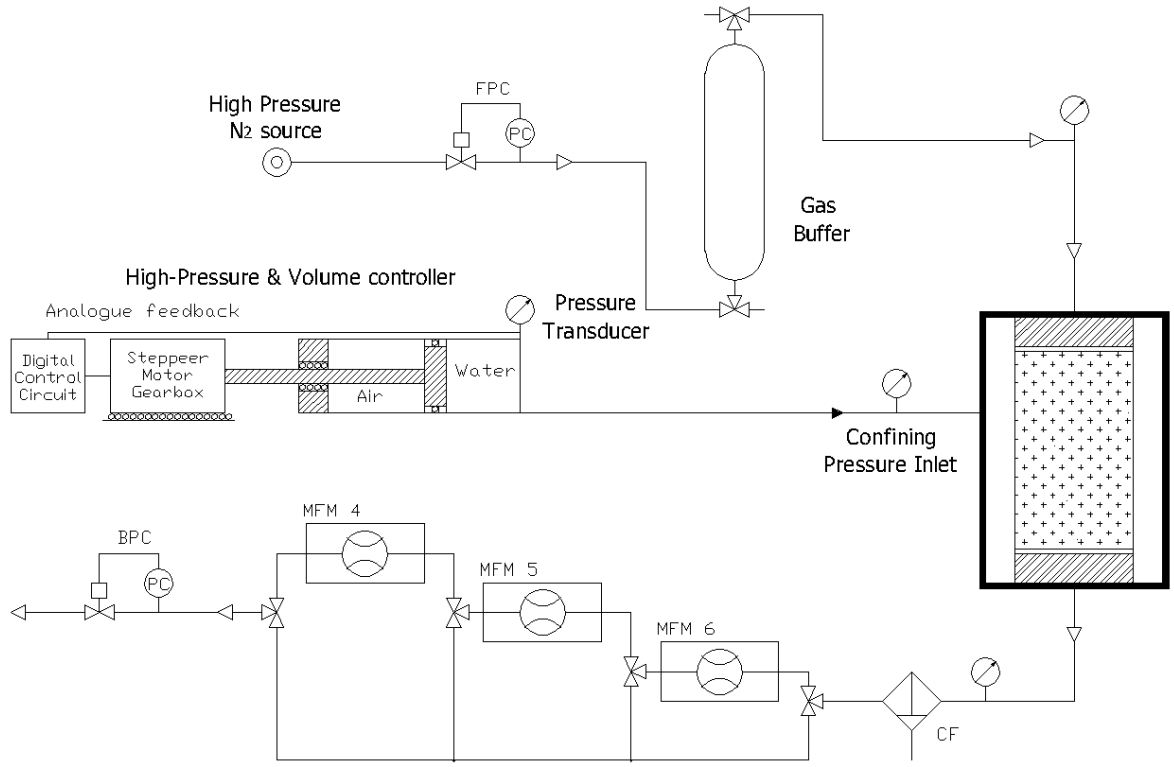


**Figure 2: Experimental setup with piston controller - low pressure line (CF: coalescing filter, FPC: forward-pressure controller, BPC: back-pressure controller, MFM: mass flow meter)**

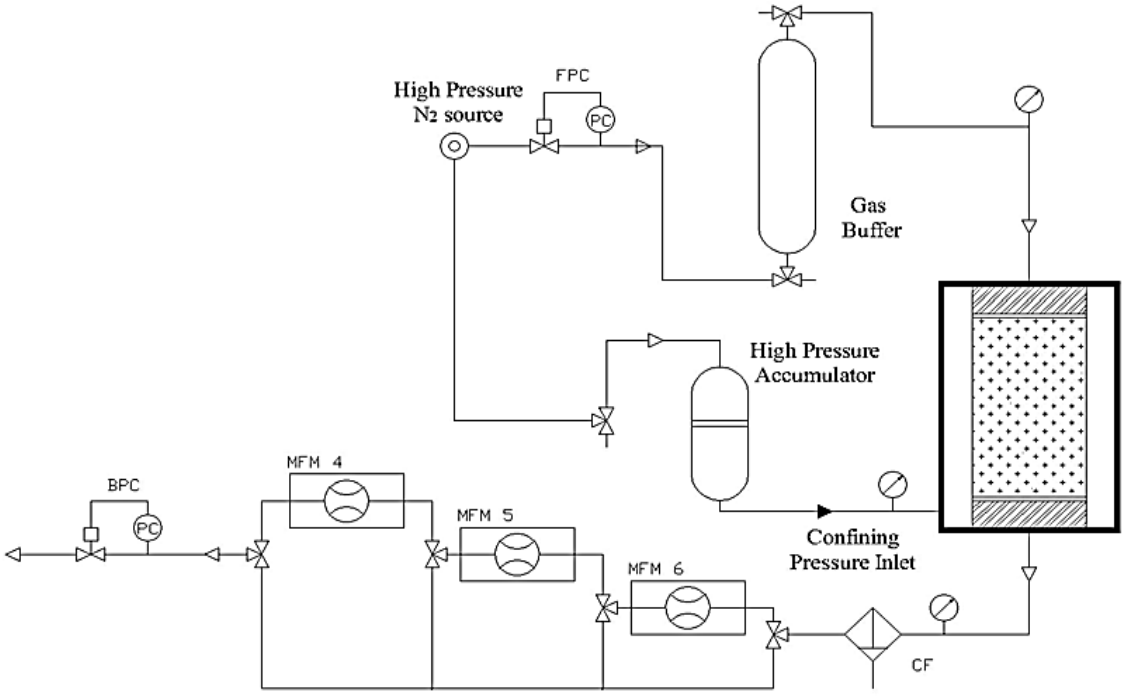


**Figure 3: Experimental setup with bladder accumulator - high pressure line (CF: coalescing filter, FPC: forward-pressure controller, BPC: back-pressure controller, MFM: mass flow meter)**

- *Water/nitrogen separator*. An OLAER's pressure bladder accumulator (up to 33 MPa) was used to apply the high confining pressures (Figure 7). The internal elastic membrane kept apart the nitrogen and the water phases of the high-pressure confining pressure system.
- *Gas mass flowmeters*. The gas outflow coming out from the bottom of the sample to the atmosphere was measured using a series of three gas-mass flowmeters with different ranges: 1000, 100 and 10 STP $cm^3$/min (the latter was 2 STP $cm^3$/min in the high-pressure line), with a turndown of 1:50 (minimum value measured with acceptable accuracy 2% FS). HI-TEC flowmeters operate on a principle of heat transfer by sensing the temperature increment along a heated section of a capillary tube. They were calibrated to the consigned conditions: nitrogen gas, pressure 70 bar a, and temperature 20°C. The output signal was 0-5 VDC.
- *Pressure transmitters*. DRUCK pressure transmitters PTX1400 were placed at the outlet port of the water/nitrogen separator (confining pressure) and the outlet of the system (atmospheric pressure). The transmitters' range was 100 bar a (0.25% BSL). The output signal was 4-20 mA.
- *Pressure sensors*. DRUCK pressure sensors UNIK 5000 series were placed at the inlet port of the triaxial cell (injection pressure). The range was 350 bar a (0.04% BSL). The output signal was 1-6 V.
- *Tubing, fitting and valves*. All the SWAGELOK fitting materials and valves were made of stainless steel, SS316. The SANVICK tubing material was SS316 1/8". The maximum leakage rate according to manufacturer was around 0.1 $cm^3$/min at 68 bar g.

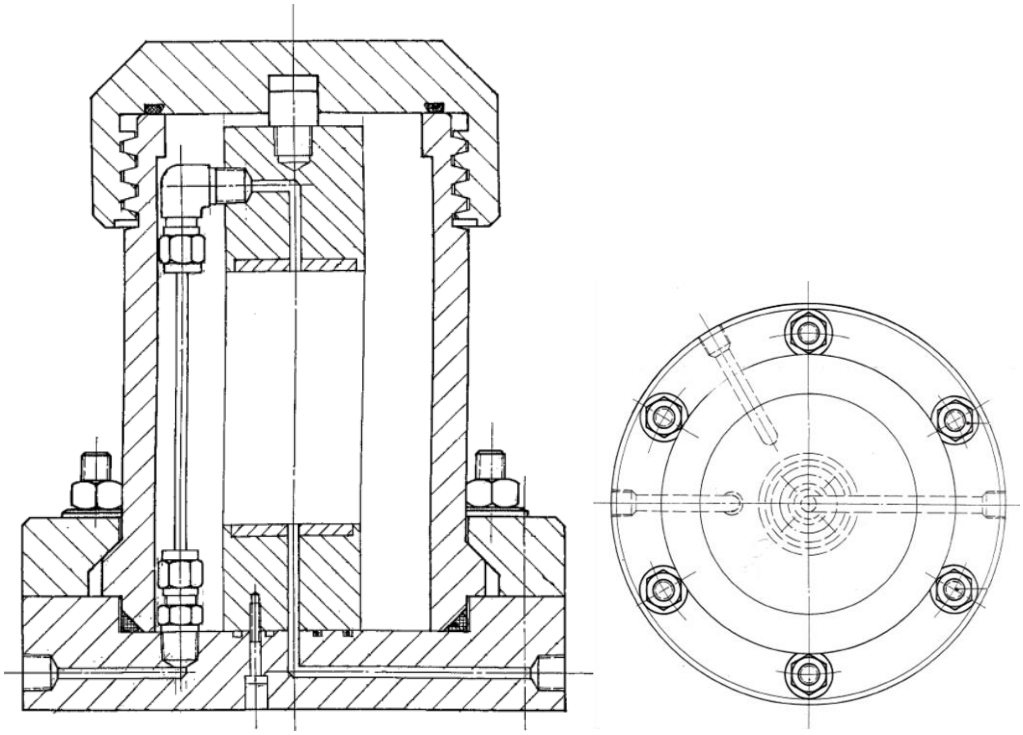

**Figure 4: Schematic design of the triaxial cell type 1 used for the gas permeability and breakthrough tests**

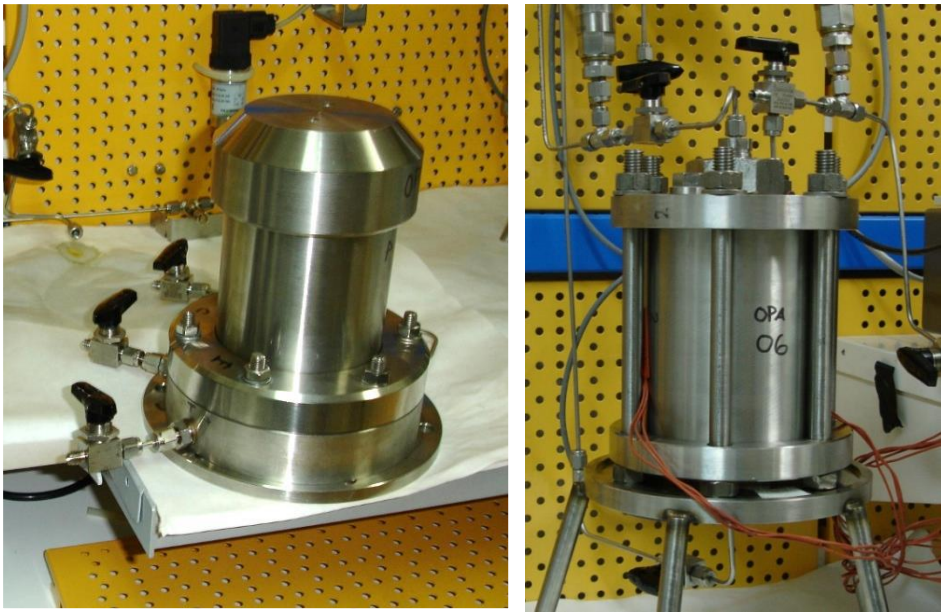


**Figure 5: Triaxial cell type 1 (left) and 2 (right)**

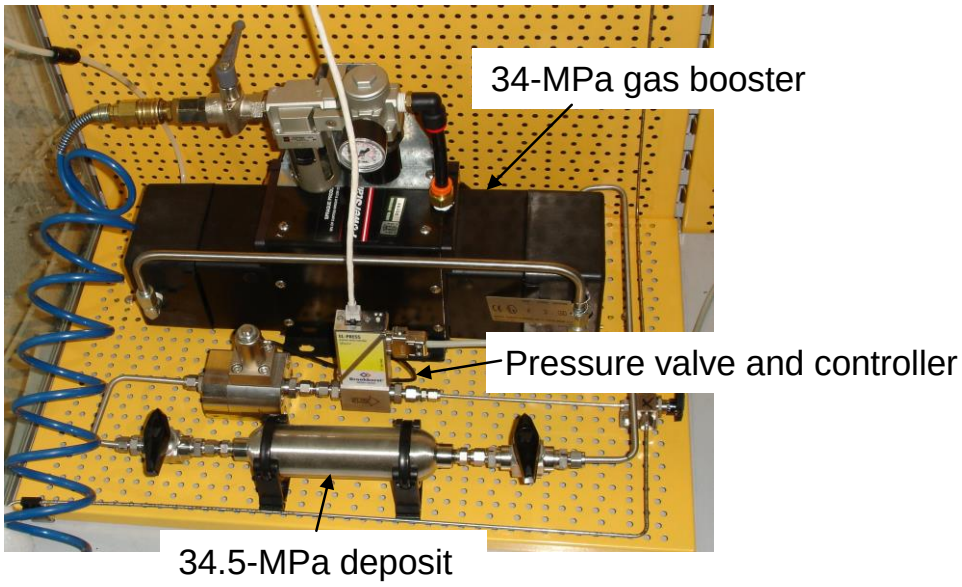


**Figure 6: Gas-booster and high-pressure deposit to supply gas to the injection pressure buffer and to the pressure accumulator applying confining pressure in the high-pressure line**

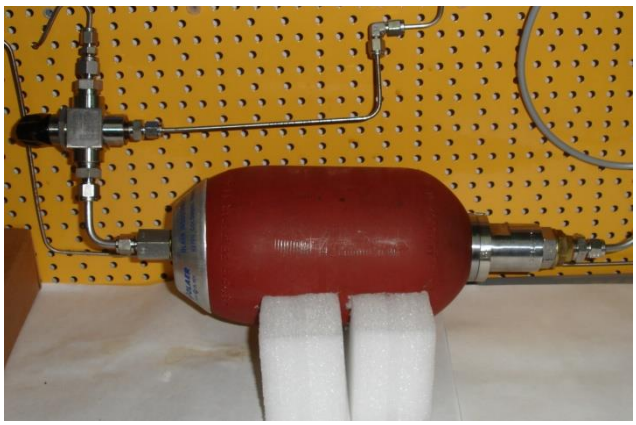

**Figure 7: Pressure accumulator to apply high confining pressure**

## 3.2 SAMPLE PREPARATION AND TEST PROCEDURE

The samples were drilled from the BDR-1 core in a sense perpendicular to bedding and they were later lathed to smooth the surface and obtain the right diameter as well as to assure the parallelism of the cylinders' ends. The resulting specimens were 1.2-3.0 cm in height and 9.2 $cm^2$ in surface area (slightly larger in tests OPA8 and OPA9). Filter paper and porous stones were placed on top and bottom of the sample. Except in tests OPA1, OPA3 and OPA5, PVC discs perforated in the middle were also placed at both ends to increase the length of the sample ensemble and improve its confinement. Samples OPA1 to OPA5 were wrapped in a rubber sleeve that shrank forming a water-resistant seal (Cold Shrink™ Connector Insulator, heat-shrink sleeve for sample OPA1) and then in a thick latex or neoprene membrane (Figure 8). Samples OPA6 to OPA9 were laterally wrapped in paraffin foil, the "sample-porous stones-PVC discs" ensemble was wrapped in duct tape and finally in the shrinking jacket (Figure 9).

**Figure 8: Appearance of an Opalinus clay sample drilled for a gas test, wrapped in the shrinking rubber sleeve (black) and in the latex membrane (red)**

**Figure 9: Opalinus clay sample placed between porous stones and perforated PVC discs, ensemble wrapped with duct tape and external shrinking jacket**

Once the triaxial cell was filled with water, it was pressurised to 8 MPa and gas was injected at a pressure of 0.5 MPa through the top of the sample. The pressure was increased by 0.5 MPa every 24 h, until reaching a value of 7 MPa. Then the cell was moved to the high-pressure line (except in tests OPA2 and OPA5), in which a confining pressure of 15 MPa was applied, either in steps or at a time. The injection pressure was also stepwise increased up to a value of 14 MPa. Then (except in tests OPA6 and OPA7), the confining pressure was increased to 19 MPa and the

injection pressure to 18 MPa, which was the maximum value allowed by the setup. In tests OPA8 and OPA9 the confining pressure was later increased above 20 MPa. The pressure paths followed in the tests are shown in Figure 10 and Figure 11. All pressure values are absolute.

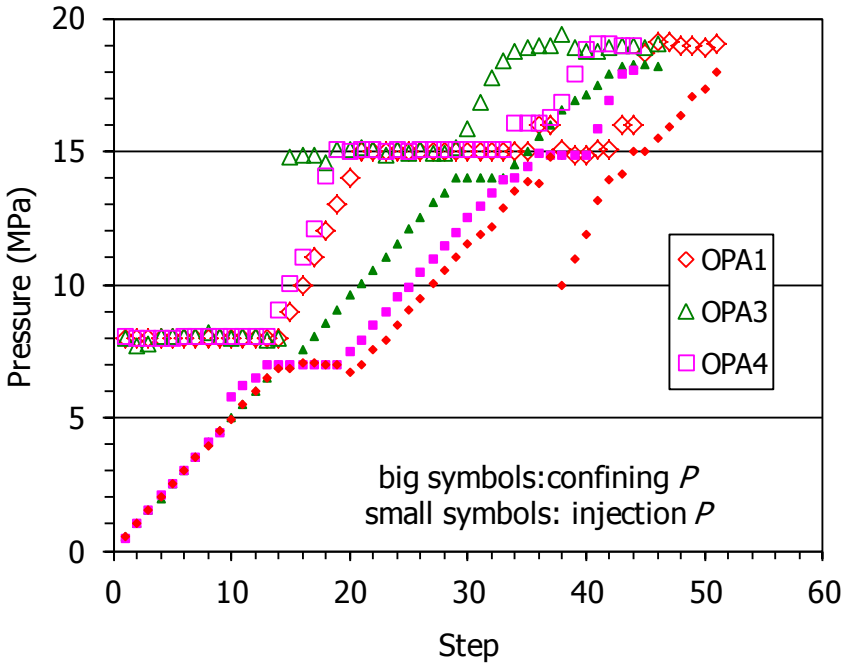


**Figure 10: Pressure paths followed in the gas breakthrough tests OPA1 to OPA5 (tests OPA2 and OPA5 followed only Phase 1 under confining pressure 8 MPa)**

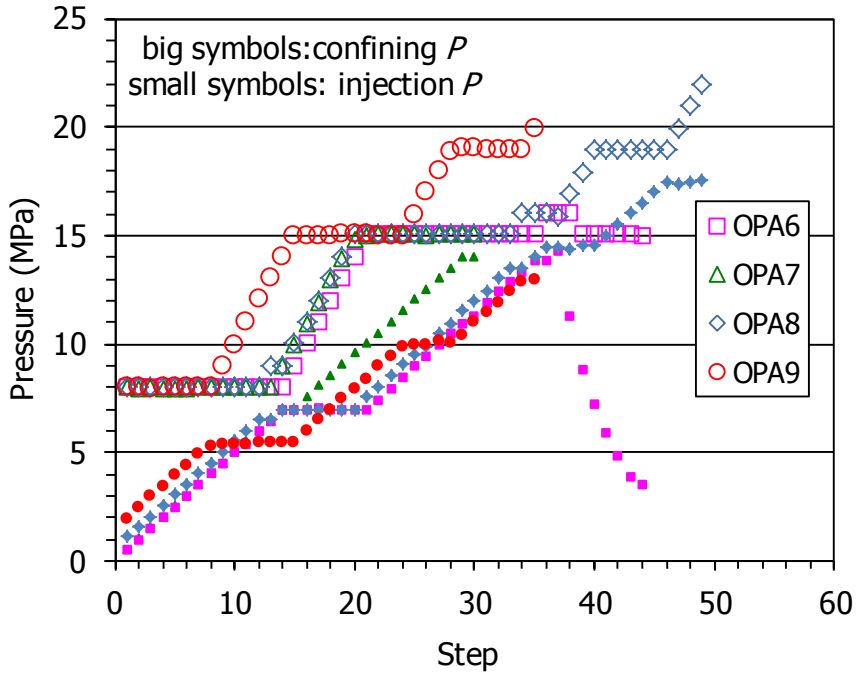


**Figure 11: Pressure paths followed in the gas breakthrough tests OPA6 to OPA9**

After the gas breakthrough tests, samples OPA3 and OPA4 were saturated with deionised water injected through the bottom surface. The sample was kept in the same triaxial cell as during the

gas permeability test, and the confining pressure applied during saturation was 1.5 MPa. After full saturation the water pressure at the bottom was increased and the backpressure was fixed on top with a GDS pressure/volume controller, which allowed to measure the water outflow and compute the hydraulic conductivity applying Darcy's law (Figure 12).

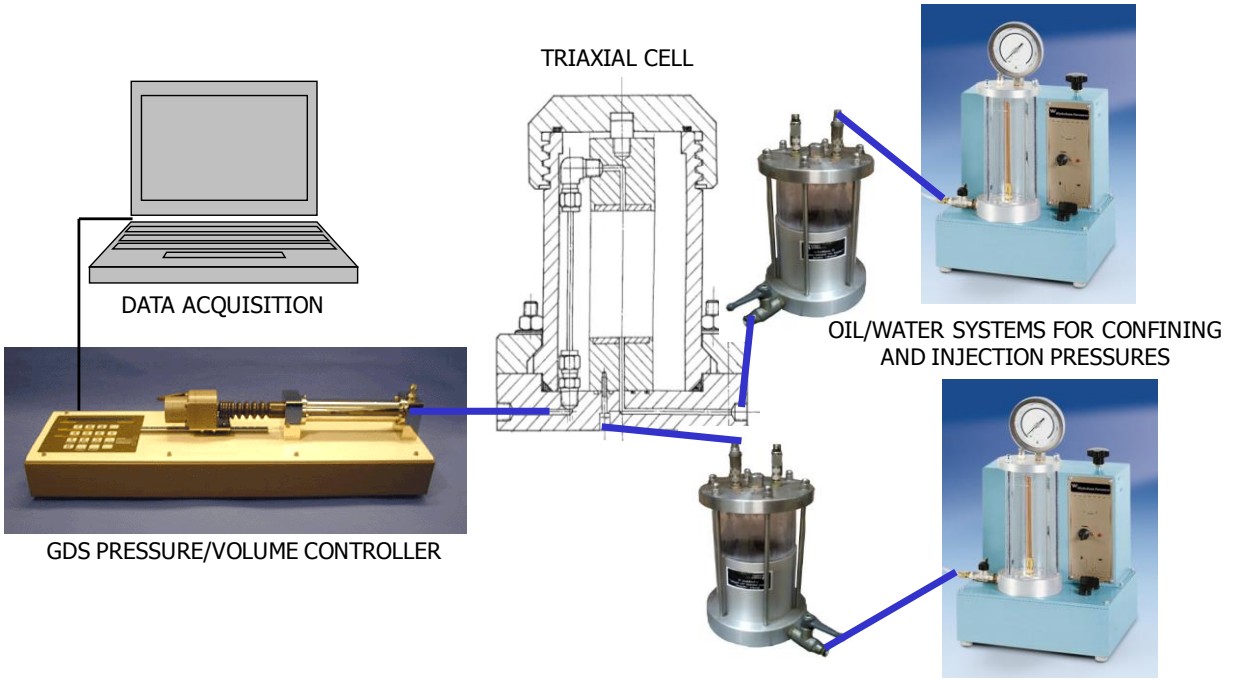


**Figure 12: Setup for the water permeability tests**

## 3.3 GAS PERMEABILITY COMPUTATION

The intrinsic permeability of the material could not be directly obtained from the measurements performed, since to determine the intrinsic permeability with air flow the sample must be completely dry. When there are two fluids present in the porous material (gas and water in this case), the permeabilities of each fluid depend on the saturation of each fluid: these are called effective permeabilities. Hence the value obtained in the determinations is the intrinsic permeability measured with gas flow, $k_{ig}$, times the relative permeability to gas, $k_{rg}$. The relative permeability to gas is the ratio of the effective permeability of gas at a particular saturation to the absolute permeability of gas at total gas saturation, i.e. in completely dry material, where the $k_{rg}$ value would be 1.

To compute the permeability the outflow measurements were used, applying the following equation for incompressible media with compressible pore fluids (Scheidegger 1974):

$$k_{ig} \cdot k_{rg} = \frac{Q_m \times \mu_g \times L \times 2P_m}{A \times (P_{up}^2 - P_{dw}^2)} \quad [1]$$

where $Q_m$ is the measured flow (volume of fluid as a function of time), $A$ is the sample surface area, $\mu_g$ is the fluid dynamic viscosity, $L$ is the sample length and $P_{up}$ and $P_{dw}$ are the upstream and downstream pressures applied at the top (inlet) and the bottom (outlet), respectively, of the sample, and $P_m$ is the pressure of the measured flow (in our case, because of the STP conditions of the gas mass flowmeters, the atmospheric pressure). In turn gas permeability, $k_g$, can be computed taking into account the gas density and viscosity change with upstream or downstream pressures ($P$):

$$k_g = \frac{\rho_g \times g \times P}{\mu_g} \times k_{ig} \times k_{rg} \quad [2]$$

It is considered that the viscosity of nitrogen did not change during the tests because they were isothermal, whereas density changed with pressure. The change in density was considered as that of an ideal gas, and thus computed as the product of the density of nitrogen at atmospheric pressure times the pressure of the flow used for the computation (*i.e*. atmospheric pressure). This solution assumed that steady state flow was established, which meant that the quantity of gas exiting the sample in the low pressure side was equal to that entering the sample in the high pressure side. In any case, the underestimation of the calculated permeability coefficients should be less than 1.3%.

# 4 Results

Nine gas permeability tests were performed in triaxial cells with Opalinus clay samples obtained by drilling from the BDR-1 core in the sense perpendicular to bedding. Care was taken to avoid density and water content changes during the preparation of the samples. The samples were not saturated before the gas injection tests, but their degree of saturation could increase during the tests because of the high confining pressures applied. Table I summarises the characteristics of the specimens used.

**Table I: Characteristics of the specimens used for the gas permeability tests**

| Test reference | Height (cm) | Surface area ($cm^2$) | Initial $\rho_d$ ($g/cm^3$) | Initial *w* (%) | Initial $S_r$ (%) | Final $\rho_d$ ($g/cm^3$) | Final *w* (%) | Final $S_r$ (%) |
|---|---|---|---|---|---|---|---|---|
| OPA1 | 3.01 | 9.05 | | | | 2.29 | 4.8 | 72 |
| OPA2 | 2.42 | 9.24 | 2.32 | 2.1 | 34 | | 5.6 | |
| OPA3 | 2.84 | 9.19 | 2.29 | 5.6 | 84 | 2.22 | 5.7 | 69 |
| OPA4 | 1.23 | 9.29 | 2.21 | 7.5 | 90 | 2.12 | 7.3[a, b] | 71 |
| OPA5 | 1.96 | 9.11 | 2.33 | 5.8 | 96 | 2.33 | 5.8 | 96 |
| OPA6 | 1.09 | 9.32 | 2.32 | 3.3 | 53 | 2.34 | 2.4 | 41 |
| OPA7 | 1.17 | 9.32 | 2.31 | 3.1 | 49 | | 6.8[b] | |
| OPA8 | 2.03 | 11.40 | 2.32 | 4.7 | 75 | 2.29 | 4.7 | 69 |
| OPA9 | 1.78 | 11.34 | 2.36 | 3.9 | 70 | 2.39 | 3.5 | 71 |
| Average | 1.95±0.71 | 9.70±0.95 | 2.31±0.04 | 4.5±1.8 | 69±22 | 2.28±0.09 | 5.2±1.6 | 70±16 |

[a] the sample was saturated between two successive gas permeability tests; [b] because of a failure the sample got wet during the gas permeability test

It must be said beforehand that in most cases the flows measured during the tests were below the turndown value of the sensors, which is the accurate detection limit of the flowmeters. The flow values measured were in fact average values obtained from around 1000 thousand data (a time-integrated value of instantaneous flow), most of which could be zero or below their turndown value. But higher flows were observed occasionally, which can be the reason why

average values higher than 0 were recorded. If these flows were considered representative of the actual flow, tentative permeability values could be computed. This has been done in those cases in which coherent flow tendencies were observed and when the pressure in the upward deposit decreased during a particular step, because this would mean (excluding gas leaks in the system) that some flow was taking place across the sample.

Depending on the flowmeter used this turndown value was different. Thus, when the 10 mL/min flowmeter was used in the low-pressure line, flow values below 0.2 mL/min can be considered uncertain, whereas when the 2 mL/min flowmeter was used in the high-pressure line, flows above 0.04 mL/min could be reliably measured. Table II summarises the experimental particularities of each test.

**Table II: Characteristics of the setups used**

| Test reference | Cell type | Date start | Pressure line | Flowmeter | Range (mL/min) | Turndown (mL/min) |
|---|---|---|---|---|---|---|
| OPA1 | 1 | Nov-11 | low | FT4 | 10 | 0.2 |
| | | Feb-12 | high | FT2 | 100 | 2 |
| OPA2 | 2 | Apr-12 | low | FT4 | 10 | 0.2 |
| OPA3 | 1 | Apr-12 | high | FT1 | 2 | 0.04 |
| OPA4 | 2 | Jun-12 | low | FT4 | 10 | 0.2 |
| | | Aug-12 | high | FT1 | 2 | 0.04 |
| OPA4-sat | 1 | Mar-13 | high | FT1 | 2 | 0.04 |
| OPA4-sat2 | 2 | Jul-13 | high | FT1 | 2 | 0.04 |
| OPA5 | 2 | Aug-12 | low | FT4 | 10 | 0.2 |
| OPA6 | 2 | Nov-12 | low | FT4 | 10 | 0.2 |
| OPA7 | 2 | Nov-12 | high | FT1 | 2 | 0.04 |
| OPA8 | 2 | Mar-13 | low | FT4 | 10 | 0.2 |
| | | May-13 | high | FT1 | 2 | 0.04 |
| OPA9 | 2 | Oct-13 | high | FT1 | 2 | 0.04 |

## 4.1 TEST OPA1

The procedure described in section 3.2 and the stress path represented in Figure 10 were followed in test OPA1. A thermoretractable tube, which needed heat to retract around the sample, was used to wrap it. The pressure evolution and the flow measured during the test are shown in Figure 13. The flow was always below the turndown value of the flowmeters, but it showed clear tendencies. As well, the injection pressure decreased for each step, which would mean that some flow was taking place, even if it was too low to be measured correctly.

Once the triaxial cell type 1 was filled with water, it was pressurised to 8 MPa and a gas injection pressure of 0.5 MPa was applied to the top of the sample and increased every 24 h (approximately). Every time the injection pressure increased, which implied a decrease in

effective pressure, the flow increased. The confining pressure decreased accidentally at time 576 h for 17 h, and this made the flow increase. When the injection pressure reached 7 MPa, the confining pressure was increased stepwise until 15 MPa. During this phase the flow decreased continuously, what could reflect the effect of confining pressure on permeability (Figure 14), except for an accidental decrease in confining pressure when it was set at 14 MPa, which triggered an increase in the gas flow. The injection pressure was subsequently increased up to 14 MPa, resulting in a progressive slight increase in flow that would be linked to the reduction in effective stress. Finally, the confining pressure was increased to 16 MPa (the maximum allowed in the low-pressure line equipment) and the injection pressure to 15 MPa. This situation was kept for 7 days. Then the cell was moved to the high-pressure line, in which a confining pressure of 15 MPa and an injection pressure of 8 MPa –that was progressively increased to 14 MPa– were applied. Finally, the confining pressure was increased to 19 MPa and the injection pressure to 18 MPa, which was the maximum value allowed by the setup. The flow was always below the turndown value of the flowmeter, but it reflected the changes in the stress conditions, decreasing with the increase in confining pressure and increasing with the reduction in effective pressure caused by the injection pressure rise.

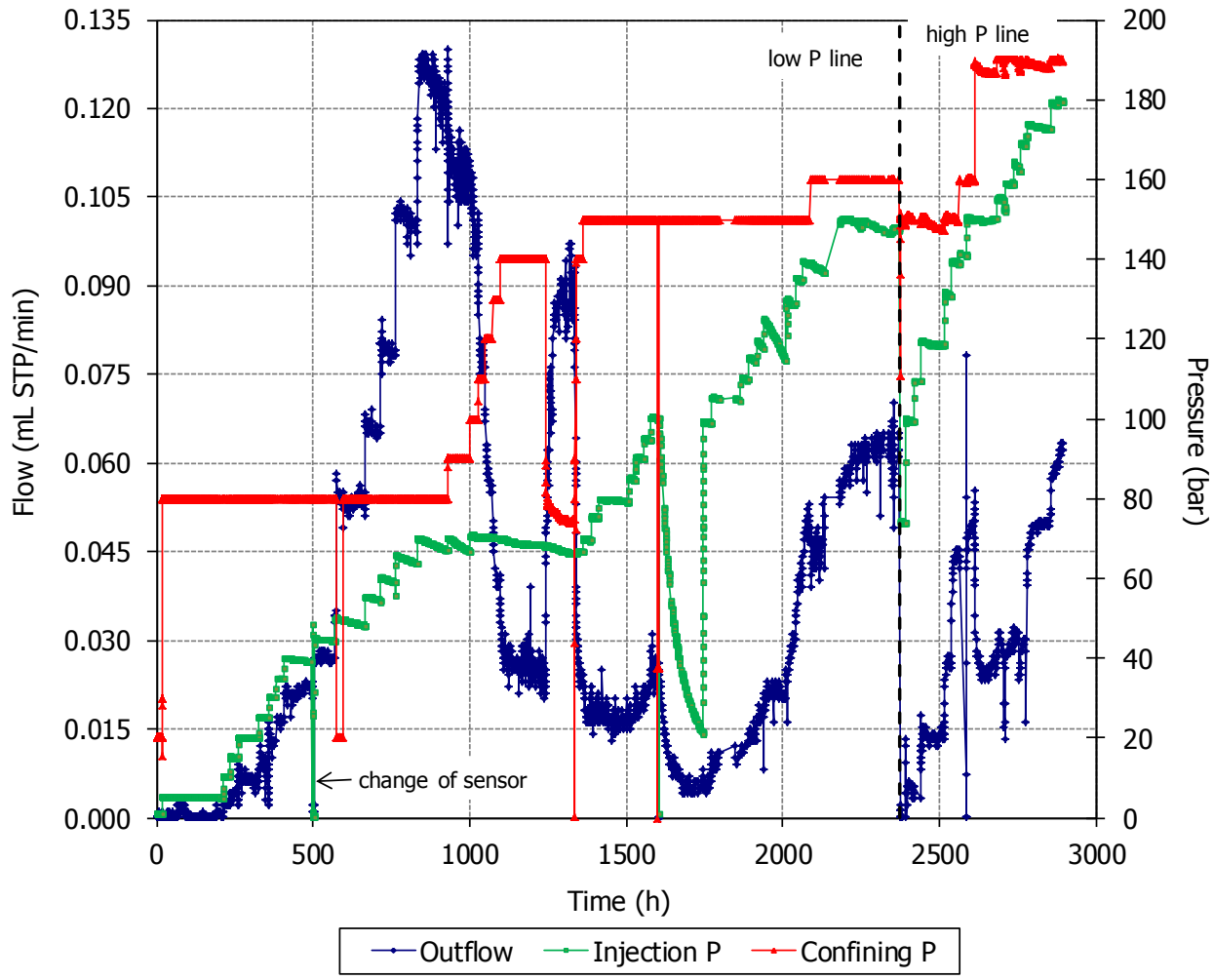


**Figure 13: Evolution of injection and confining pressure and outflow in test OPA1**

The tentative permeabilities computed from these flows are plotted in Figure 15. For the same effective pressure the permeability was lower as the confining pressure was higher. However,

the permeability increased with the decrease in effective pressure (increase in injection pressure). Again, these values should not be taken as quantitatively valid, they give just qualitatively trends.

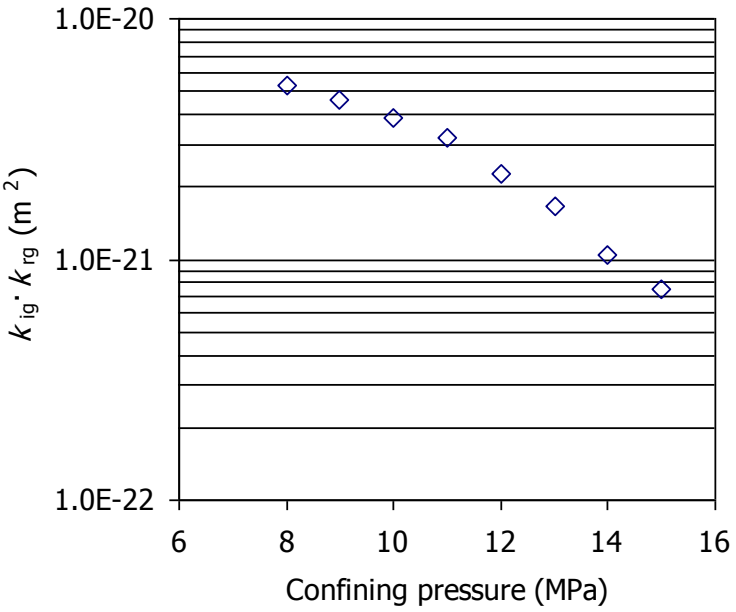


**Figure 14: Change of gas permeability with the increase of confining pressure for an injection pressure of 7 MPa and atmospheric backpressure in test OPA1 (tentative values)**

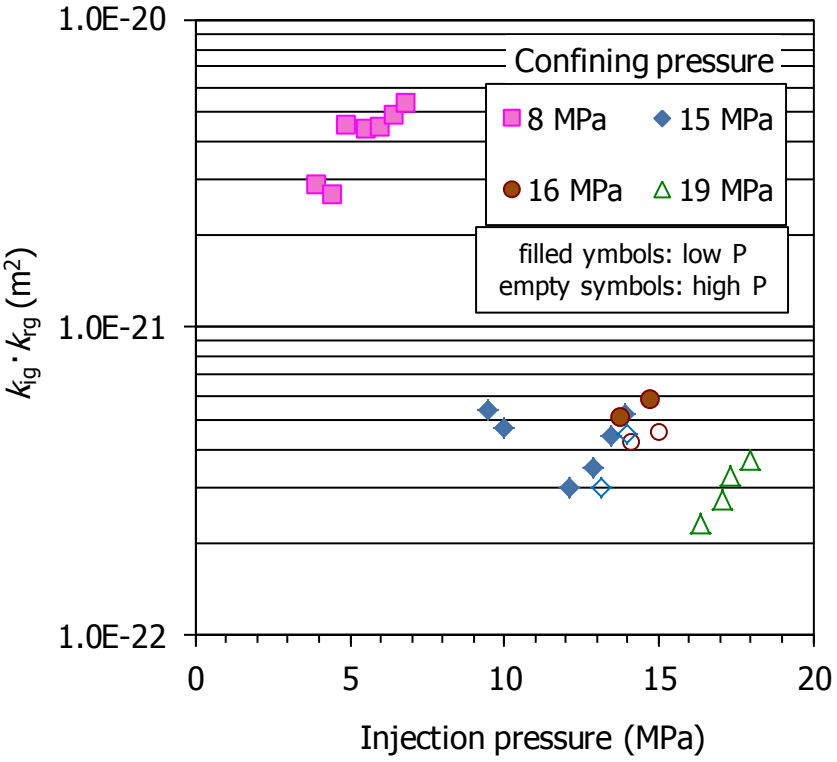


**Figure 15: Gas permeability measured for different confining and injection pressures in test OPA1 (low- and high-P lines), with atmospheric backpressure (tentative values)**

Upon dismantling the sample appeared consistent (Figure 16). It was observed under a stereomicroscope NIKON SMZ 1500. No significant features could be detected, except for a carbonate vein on the upper surface that did not have continuity in depth (Figure 17, left). However, there was a fissure along the calcite vein that could have acted as a preferential gas pathway.


**Figure 16: Final appearance of sample OPA1**

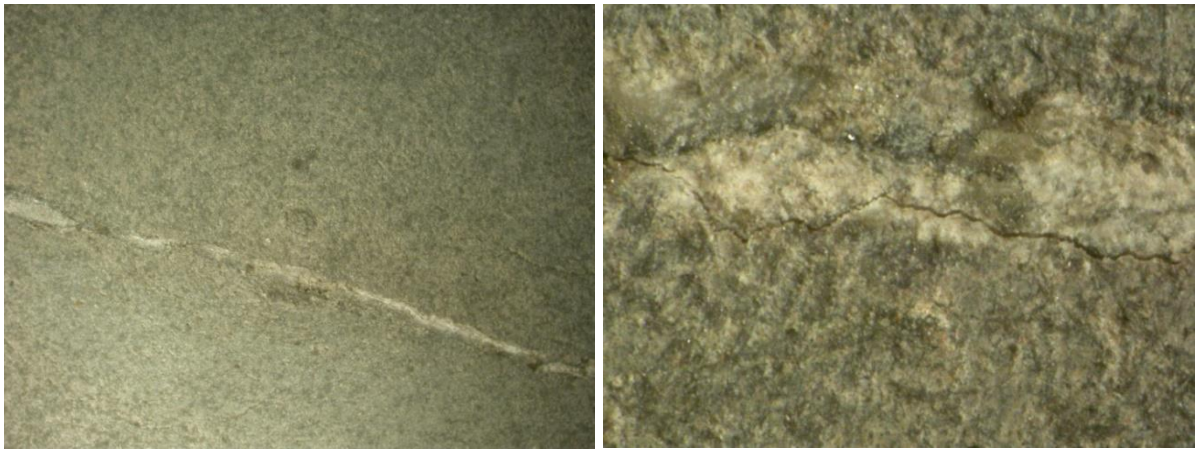

**Figure 17: Final appearance of OPA1 under the stereomicroscope (magnification of 112.5)**

## 4.2 TEST OPA2

The sample was sandwiched between porous stones and PVC perforated discs and the ensamble was placed in a triaxial cell type 2, which was filled with water and pressurised to 8 MPa. The procedure described in section 3.2 and the stress path represented in Figure 10 were followed in test OPA2. A gas injection pressure of 0.5 MPa was applied to the top of the sample and increased every 24 h (approximately) by 0.5 MPa until reaching 7 MPa. The pressure evolution and the flow measured during the test are shown in Figure 18. The flows measured were below the turndown value of the flowmeter used (0.2 mL/min) and consequently no meaningful permeability can be computed. When the confining pressure was increased to 15 MPa the membrane covering the specimen was perforated and the test had to be suspended. This perforation could be related to a lateral notch initially present in the sample, and as a result of it the sample became completely damaged (Figure 19) and the final dry density could not be determined.

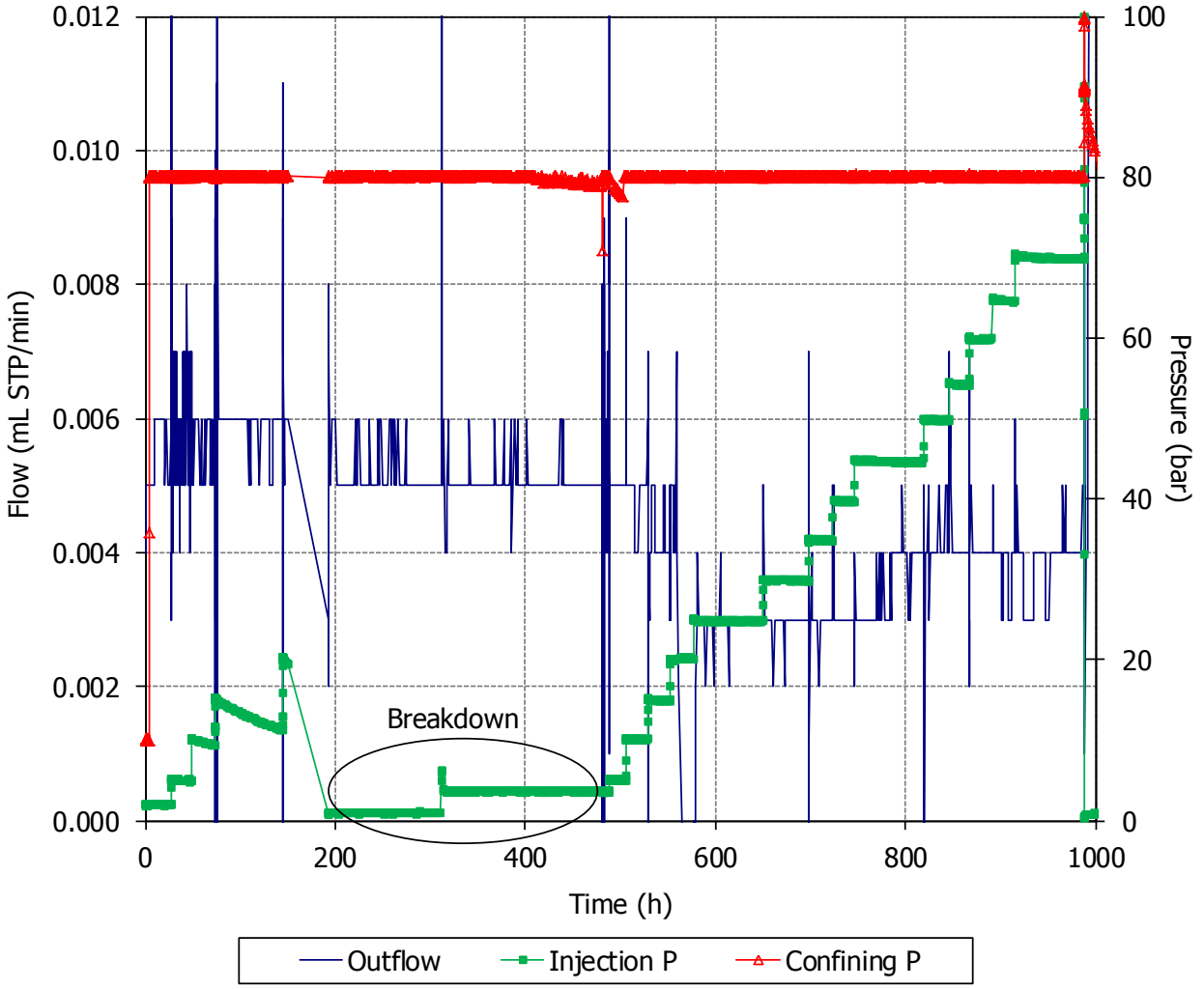


**Figure 18: Evolution of injection and confining pressure and outflow in test OPA2 (low-pressure line)**

**Figure 19: Initial and final appearance of sample OPA2**

## 4.3 TEST OPA3

The procedure described in section 3.2 and the stress path represented in Figure 10 were followed in test OPA3. This sample (Figure 20) was mounted in the triaxial cell type 1 which was initially set in the high-pressure line, for which reason the control of the confining pressure was

less steady. The pressure evolution during the test and the flow measured are shown in Figure 21. Initially the cell was pressurised to 8 MPa and a gas injection pressure of 0.5 MPa was applied to the top of the sample and increased every 24 h (approximately). When the injection pressure reached 7 MPa, the confining pressure was increased to 15 MPa. The injection pressure was subsequently increased until 14 MPa, resulting in a progressive increase in flow that would be linked to the reduction in effective stress. Afterwards, the confining pressure was stepwise increased to 19 MPa and the injection pressure to 18 MPa. This last pressure situation was kept for 27 days.

The flows measured during the test (time-integrated value of instantaneous flow) were always very low, in most of the cases below the turndown value (accurate detection limit) of the flowmeters, for which reason they can only be used as a qualitative indicator of the actual gas flow and the gas permeability values computed are only tentative. Nevertheless, the flow slightly reflected the changes in the stress conditions, tending to decrease with the increase in confining pressure and to increase with the reduction in effective pressure caused by the injection pressure rise. The slight changes in flow were not reflected in the computed permeabilities, which were very similar all along the test and seemed to be more affected by temperature changes (Figure 22). Thus, a noticeable flow increase coincided with a significant increase in the lab temperature caused by a failure in the air conditioning system (average $T$=31°C).

At the end of the test, when the effective pressure was low, “steady” gas flow (although one order of magnitude below the limit of the flowmeter accuracy) was recorded. This could be related to the formation of gas pathways that remained later open.

**Figure 20: Appearance of specimen OPA3 after drilling from the core**

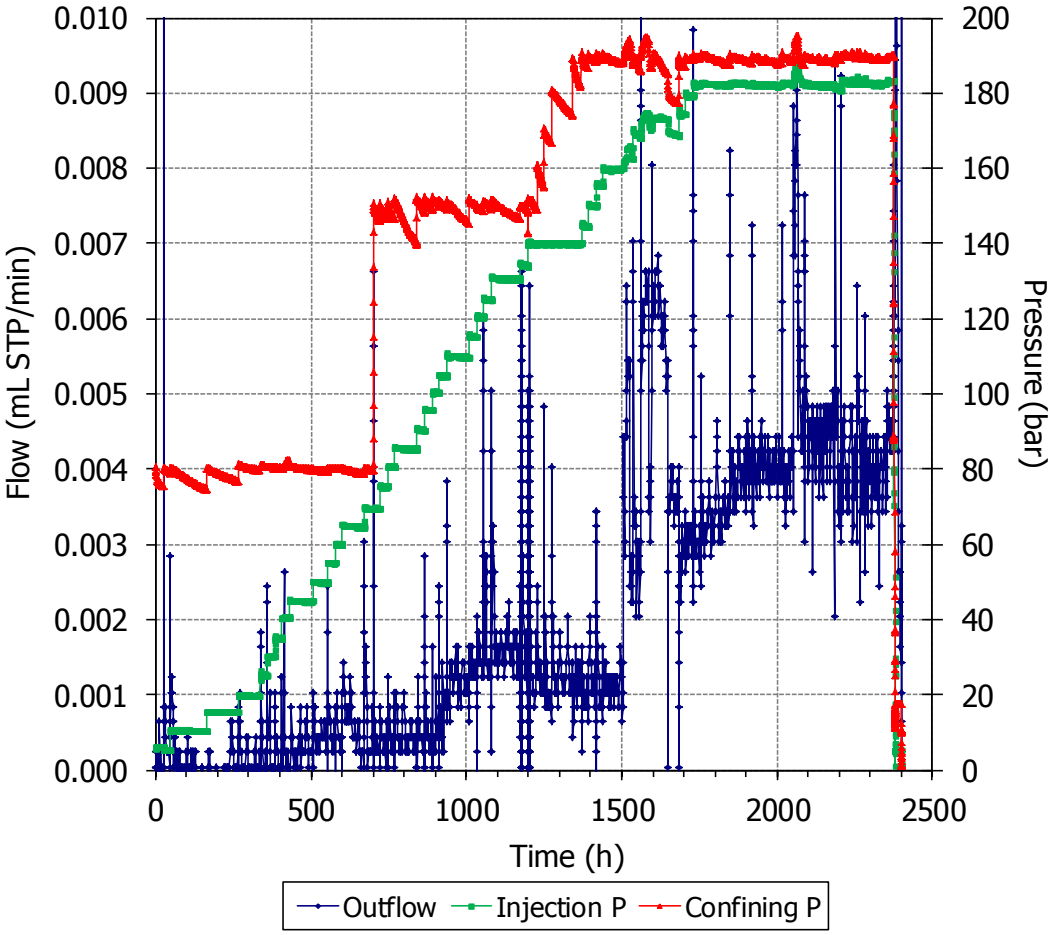


**Figure 21: Evolution of injection and confining pressure and outflow in test OPA3 (high-pressure line)**

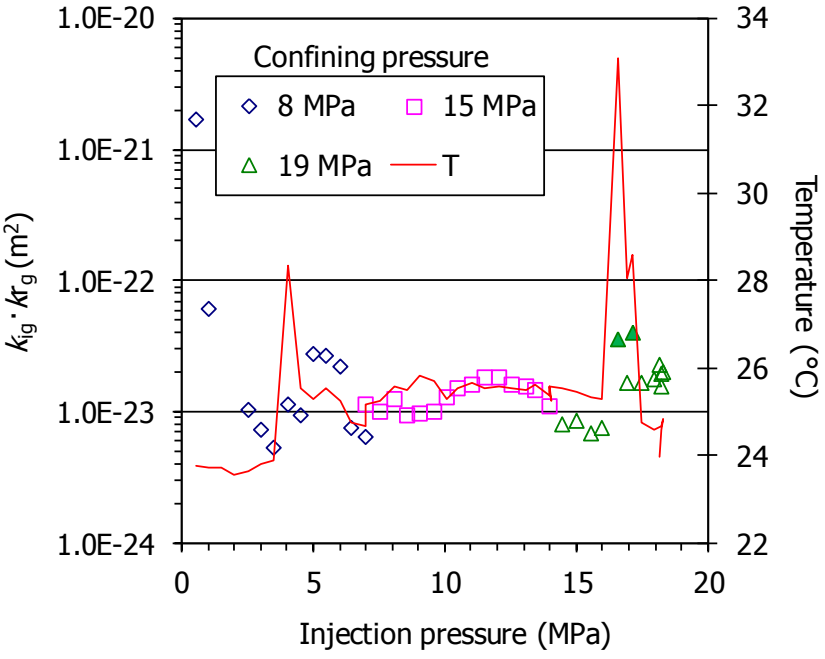


**Figure 22: Change of gas permeability with the increase of injection pressure for different confining pressures and atmospheric backpressure in test OPA3 (tentative values)**

After the gas permeability test, the same cell was moved to a water constant head permeameter (Figure 12), a confining pressure of 0.8 MPa was applied and the sample was hydrated with deionised water injected through the bottom surface at a pressure of 0.6 MPa for 78 days. After saturation the confining pressure was increased to 1.5 MPa, the water pressure at the bottom was increased to 1.2 MPa and a backpressure of 0.6 MPa was applied on top. The water outflow in the direction perpendicular to bedding was measured and the permeability computed applying Darcy's law. The results obtained are shown in Table III. The final dry density measured was lower than the initial, which could be due to the decompression occurred on releasing the confining pressure.

**Table III: Characteristics of the water permeability test in sample OPA3 (confining *P*=1.5 MPa)**

| Initial $\rho_d$ (g/cm$^3$) | Initial *w* (%) | Initial $S_r$ (%) | Hyd. grad. | *t* (days) | $k_w$ (m/s) | $k_i$ (m$^2$) | Final $\rho_d$ (g/cm$^3$) | Final *w* (%) | Final $S_r$ (%) |
|---|---|---|---|---|---|---|---|---|---|
| 2.22 | 5.7 | 69 | 2043 | 6 | $2.2\cdot10^{-13}$ | $2.3\cdot10^{-20}$ | 2.18 | 8.4 | 94 |

## 4.4 TEST OPA4

The sample was sandwiched between porous stones and PVC perforated discs and the ensamble was placed in a triaxial cell type 2. The procedure described in section 3.2 and the stress path represented in Figure 10 were followed in test OPA4. The pressure evolution during the test and the flow measured are shown in Figure 23. Initially the cell was pressurised to 8 MPa and a gas injection pressure of 0.5 MPa was applied to the top of the sample and increased every 24 h (approximately). When the injection pressure reached 7 MPa, the confining pressure was increased stepwise to 15 MPa. The injection pressure was subsequently increased also stepwise up to 14 MPa. Afterwards, the confining pressure was increased to 16 MPa and the injection pressure to 15 MPa and these values were kept for 9 days. After changing the cell to the high-pressure line, the confining pressure was increased stepwise up to 19 MPa while the injection pressure was kept at 15 MPa. Afterwards the injection pressure was progressively increased to 18 MPa (the maximum allowed by the setup). This last pressure situation was kept for 47 days.

The flows measured were always very low, below the turndown value of the flowmeters, both in the low and in the high-pressure lines. When moved to the high-pressure line, the flow values showed less noise and an overall lower value, because of the different range of the flowmeters used in the two lines (10 *vs*. 2 cm$^3$ STP/min). In both cases, gas flow showed spikes. Hence, the gas permeability values computed are not reliable, although they show a trend to decrease as the confining and injection pressures were higher (Figure 24).

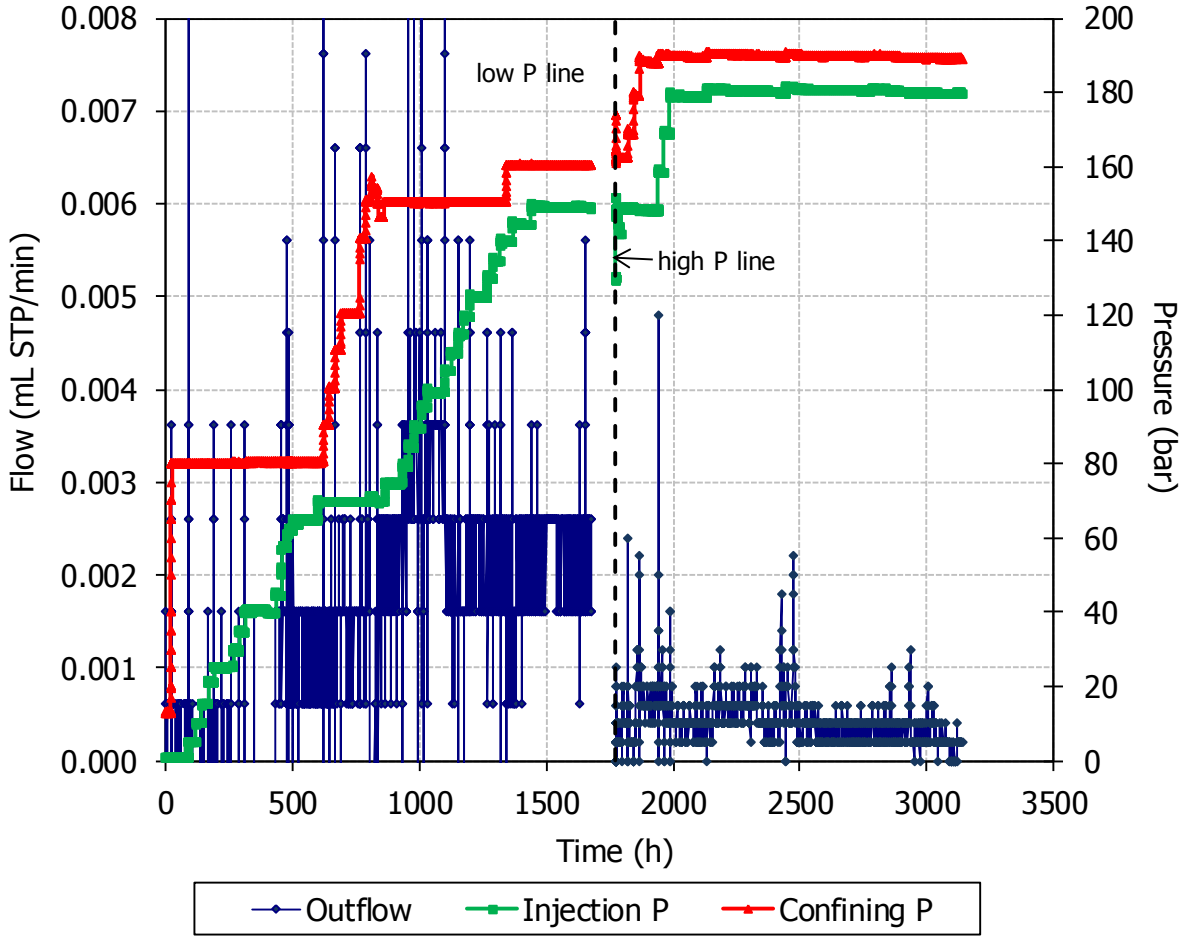


**Figure 23: Evolution of injection and confining pressure and outflow in test OPA4**

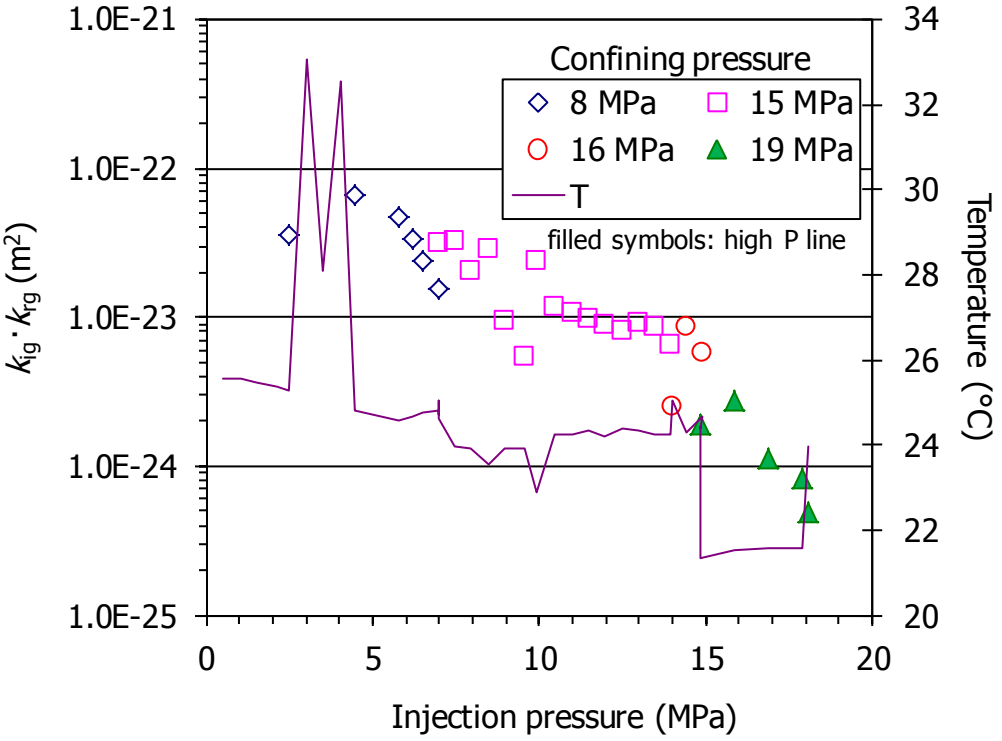


**Figure 24: Change of gas permeability with the increase of injection pressure for different confining pressures and atmospheric backpressure in test OPA4 (uncertain values)**

After the gas permeability test, the same cell was moved to a water constant head permeameter (Figure 12) and the sample was hydrated under a confining pressure of 1.5 MPa with deionised water injected through the bottom surface at a pressure of 0.6 MPa for 65 days, while the upper outlet was kept closed. Afterwards the water pressure at the bottom was increased to 1.0 MPa and a backpressure of 0.4 MPa was applied on top and the water outflow measured. Previously the injection pressure had been set to 0.6 and 0.8 MPa, but no flow had been obtained under these hydraulic gradients (1560 and 3144, respectively). Once steady flow was attained, the hydraulic conductivity was computed applying Darcy's law. The results obtained are shown in Table IV. The final dry density measured was lower than the initial, which could be due to the decompression occurred on releasing the confining pressure and would explain why the final degree of saturation is lower than 100%.

**Table IV: Characteristics of the water permeability test in sample OPA4 (confining *P*=1.5 MPa)**

| Initial $\rho_d$ (g/cm$^3$) | Initial *w* (%) | Initial $S_r$ (%) | Hyd. grad. | *t* (days) | $k_w$ (m/s) | $k_i$ (m$^2$) | Final $\rho_d$ (g/cm$^3$) | Final *w* (%) | Final $S_r$ (%) |
|---|---|---|---|---|---|---|---|---|---|
| 2.19 | 6.8 | 78 | 4672 | 23 | $2.7\cdot10^{-14}$ | $2.7\cdot10^{-21}$ | 2.12 | 8.9 | 86 |

After the hydraulic conductivity measurement the sample was again tested in the gas permeability setup in cell type 1. The same pressure path was followed as in the previous measurement, but a failure in the system occurred when the confining pressure was 15 MPa and the injection pressure 7.5 MPa and the cell had to be dismounted. The pressures and flow evolution until that moment are shown in Figure 25. Taking into account that the flowmeter used had a turndown value of 0.2 mL/min, it can be considered that the values recorded were not significant and that no flow took place.

After the failure the sample was kept in paraffin foil to avoid water losses and the same sample was mounted 3 months later in cell type 2. This cell was modified so that to avoid the displacement of the upper piston caused by the high isostatic pressure (Figure 26). The pressure and flow evolution of this second try are shown in Figure 27. No significant flow was measured in all this process, since the values recorded were below the turndown value of the flowmeter (0.2 mL/min). Besides the pressure in the upwards deposit kept constant during each step, which would be an additional indication of lack of flow. Hence, it can be considered that, as in the previous attempt, no flow took place and consequently the gas permeability of the sample reduced after saturation.

Upon dismantling the sample appeared fractured along a stratification plane in two parts (Figure 28).

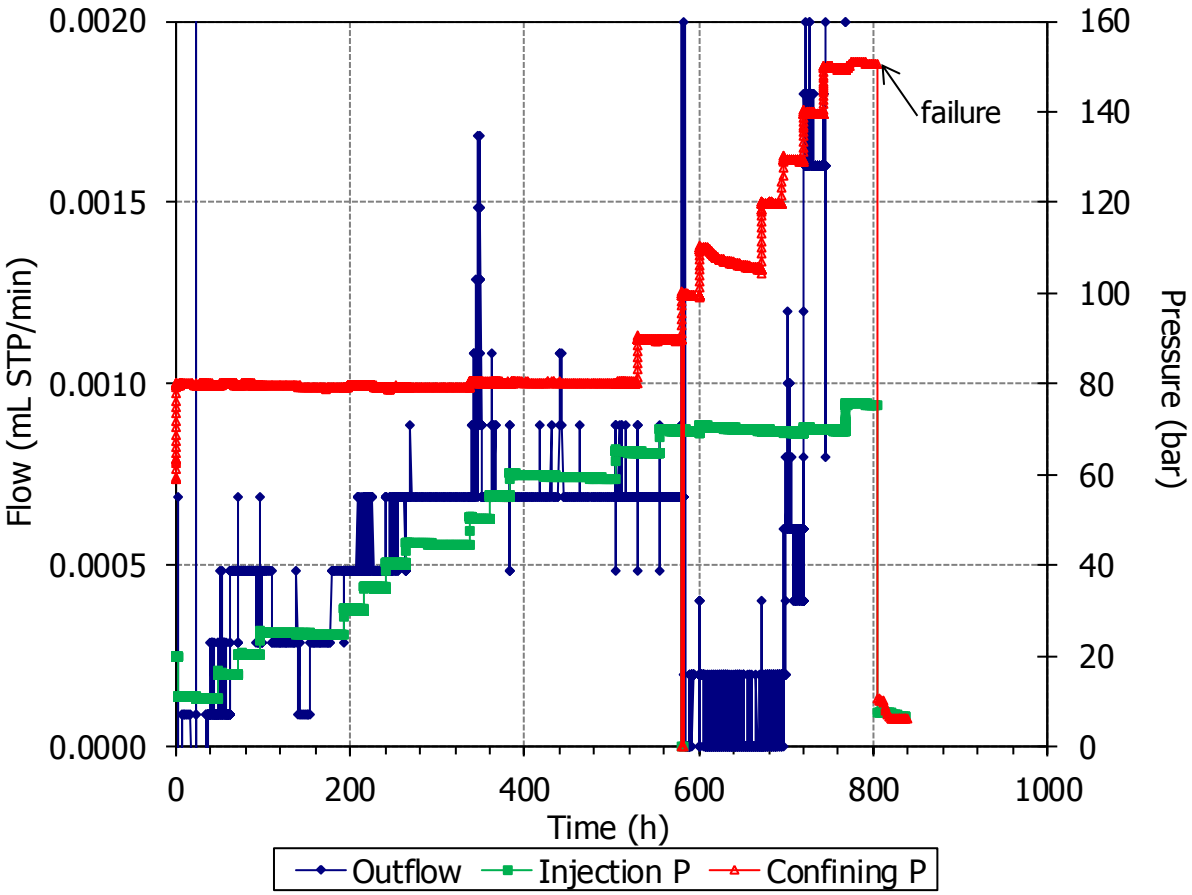


**Figure 25: Evolution of injection and confining pressure and outflow in test OPA4 after saturation (cell type 1, low-pressure line)**


**Figure 26: Sample OPA4 mounted in cell type 2 modified to avoid vertical displacement**

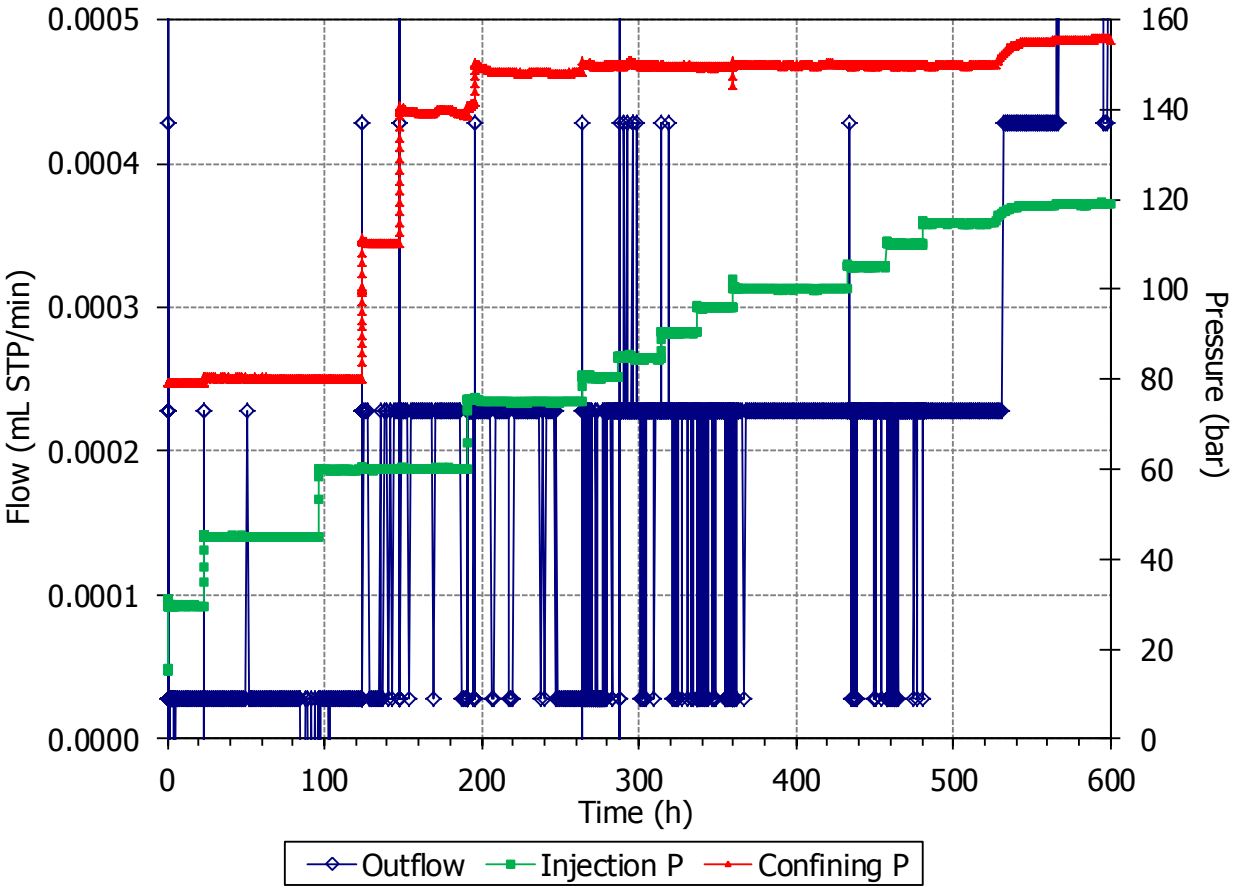


**Figure 27: Evolution of injection and confining pressure and outflow in test OPA4 after saturation and failure (cell type 2, low-pressure line)**

**Figure 28: Final appearance of sample OPA4**

## 4.5 TEST OPA5

The procedure described in section 3.2 and the stress path represented in Figure 10 were followed in test OPA5. This sample was mounted in the triaxial cell type 2 sandwiched between porous stones. The triaxial cell was filled with water and pressurised to 8 MPa. A gas injection pressure of 0.5 MPa was applied to the top of the sample and increased every 24 h (approximately) by 0.5 MPa. The pressure evolution and the flow measured during test OPA5 are shown in Figure 29. The flows measured were very low, two orders of magnitude lower

than the turndown value of the flowmeter used (0.2 mL/min), hence no significant permeability values could be computed. When the injection pressure was increased to 6 MPa the membrane covering the specimen was pierced and the test had to be suspended because the sample became completely damaged (Figure 30).

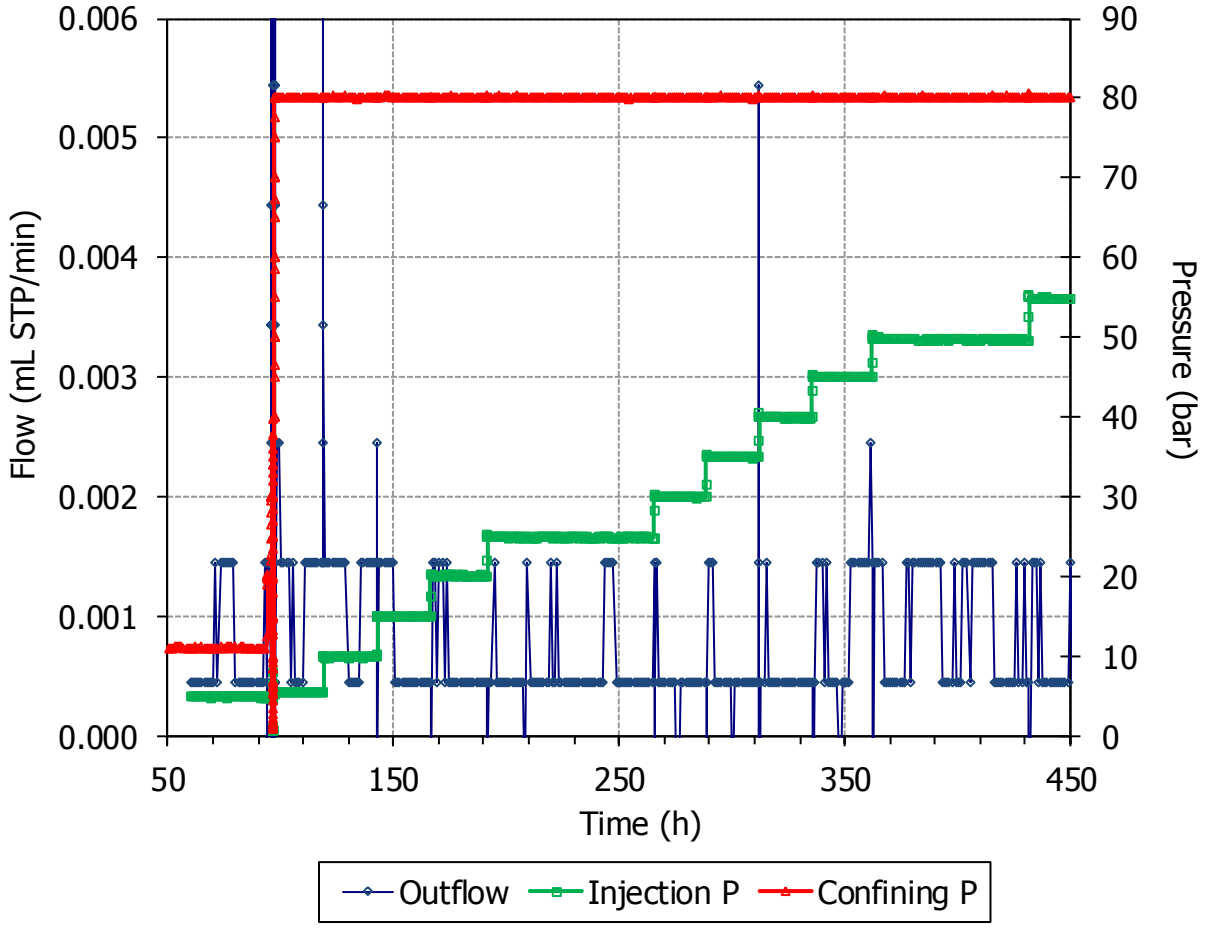


**Figure 29: Evolution of injection and confining pressure and outflow in test OPA5 (low-pressure line)**

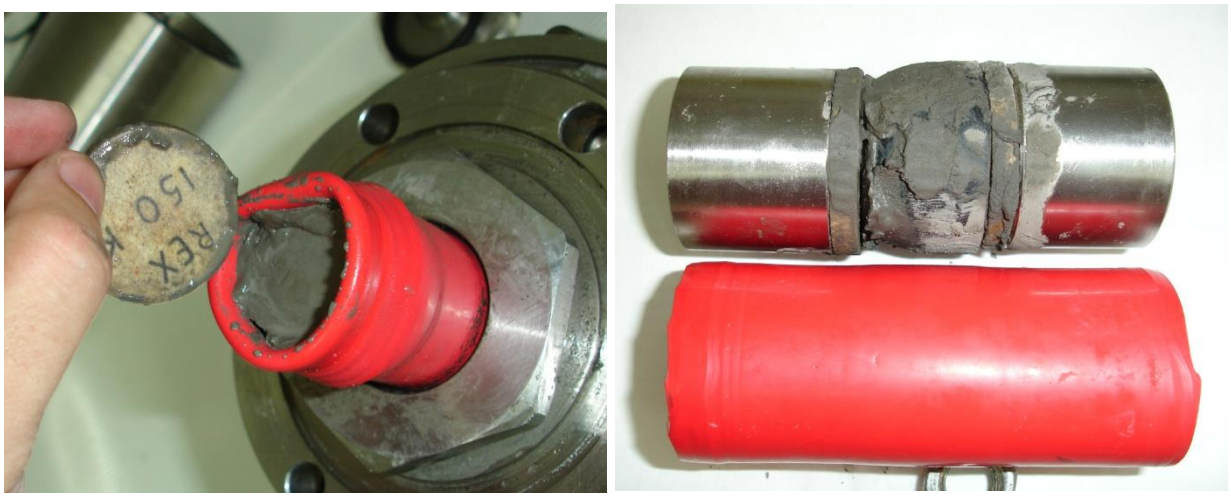

**Figure 30: Final appearance of specimen OPA5**

## 4.6 TEST OPA6

The procedure described in section 3.2 and the stress path represented in Figure 11 were followed in test OPA6. This sample was mounted in the triaxial cell type 2, sandwiched between porous stones and two PVC perforated cylinders to fit the internal dimensions of the cell (Figure 31). The pressure path and the flow measured during test OPA6 are shown in Figure 32. The triaxial cell was filled with water and pressurised to 8 MPa in the low-pressure line. A gas injection pressure of 0.5 MPa was applied to the top of the sample and increased every 24 h (approximately) by 0.5 MPa. Once the injection pressure reached 7 MPa, the confining pressure was increased to 15 MPa in 1-MPa steps. This confining pressure value was kept and the injection pressure was increased in 0.5-MPa steps until 15 MPa. When the injection pressure reached 12 MPa there was a sudden increase in flow that kept higher for the rest of the test, never stabilising after each pressure increase. The flows measured until then were below the turndown value of the flowmeter used (0.2 mL/min), hence the permeability values computed from them are uncertain. Nevertheless they have been plotted in Figure 33, where the decrease in permeability with the increase in injection pressure can be observed. This was not to be expected beforehand, since the increase in injection pressure under constant confining stress implied a decrease in effective stress and in fact a flow increase. It must be taken into account that for the computation of permeability the injection pressure is also considered (Equation 1), and its increase implied a decrease in permeability that could not be compensated by the associated flow increase recorded, which was very low. The permeabilities computed during the phase in which the injection pressure was 6 MPa and the confining pressure increased from 8 to 15 MPa barely changed and were around $1 \cdot 10^{-21}$ $m^2$ (tentative value). The few reliable permeability values computed were on average $2.5 \cdot 10^{-21}$ $m^2$ and independent of the injection pressure (in the range 12-14 MPa) and of the confining pressure (15-16 MPa). Finally the confining pressure was increased to 16 MPa and the injection pressure to 15 MPa. For this pressure situation the neoprene jacket of the sample slit and the test had to be terminated (Figure 34).

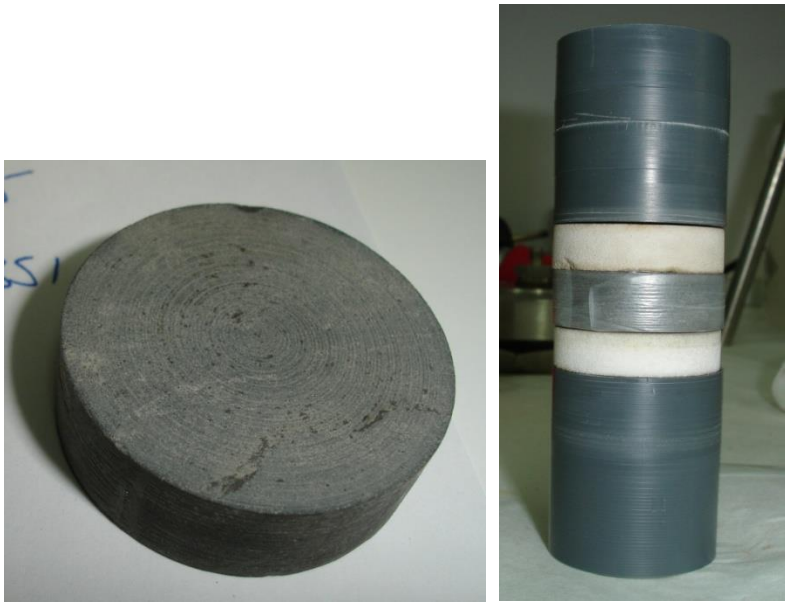

**Figure 31: Initial appearance of sample OPA06**

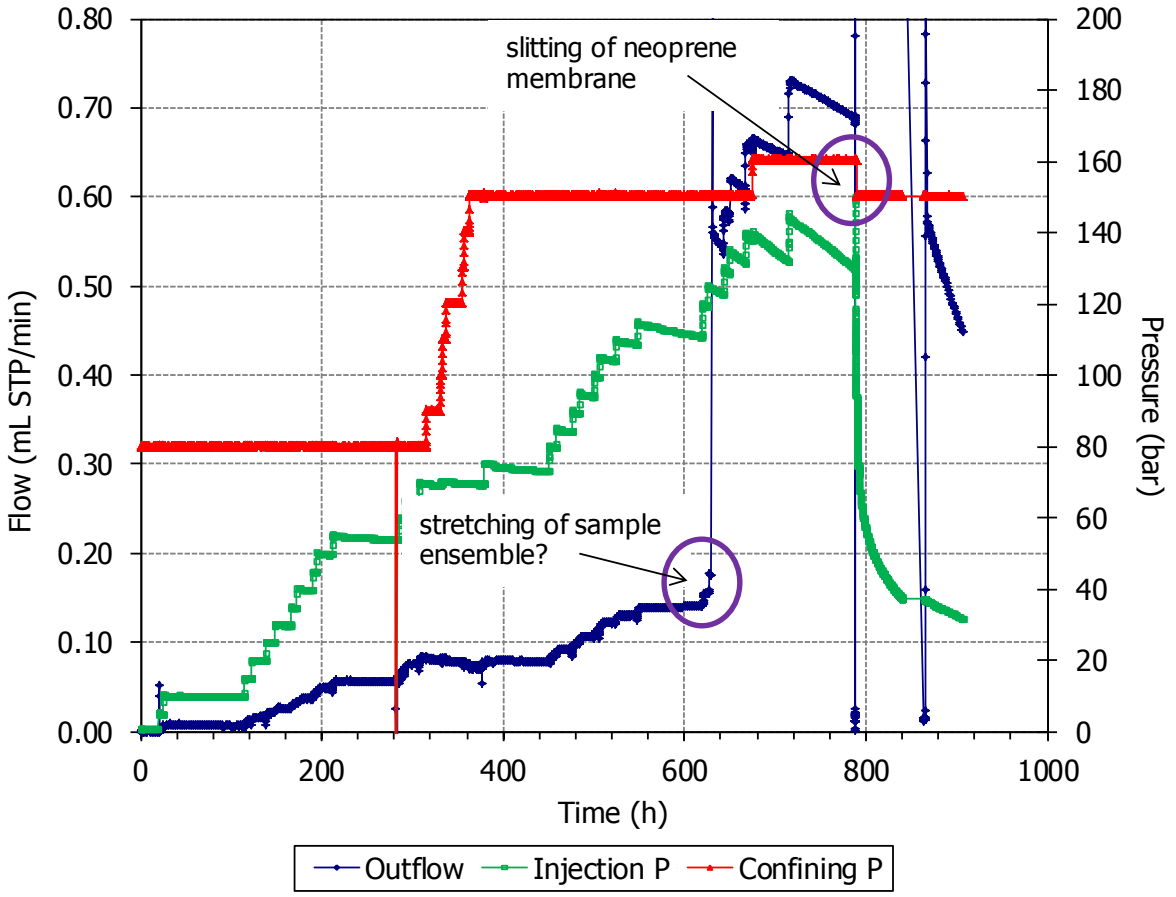


**Figure 32: Evolution of injection and confining pressure and outflow in test OPA6 (low-pressure line, cell 2)**

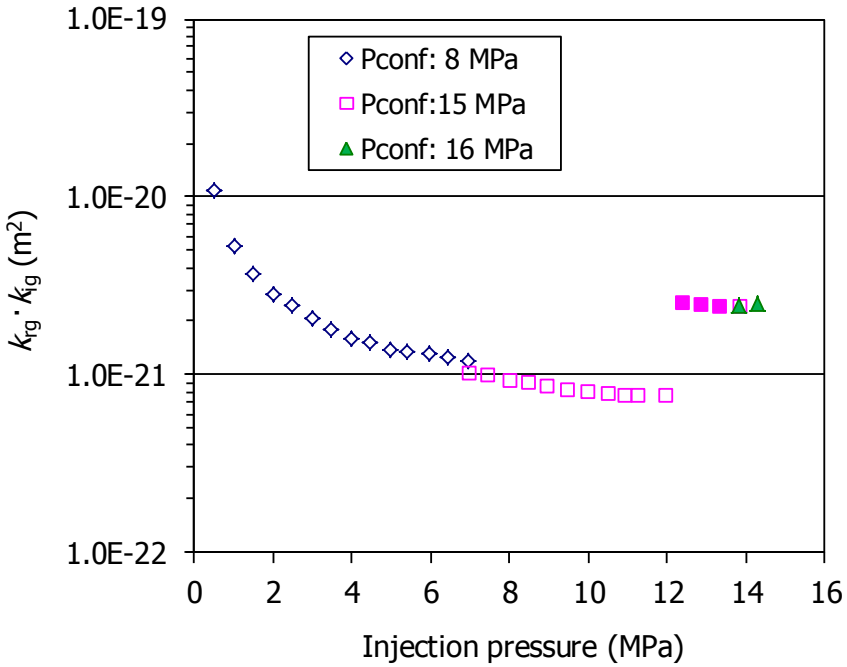


**Figure 33: Change of gas permeability with the increase in injection pressure for confining pressures 8 and 15 MPa and atmospheric backpressure in test OPA6 (the empty symbols are uncertain values)**

**Figure 34: Final appearance of the sample ensemble in test OPA6, with the slit membrane**

## 4.7 TEST OPA7

The procedure described in section 3.2 and the stress path represented in Figure 11 were followed in test OPA7. This sample was mounted in the triaxial cell type 2, exactly in the same way as sample OPA6 (Figure 31), although it was pressurised through the high-pressure line. The pressure evolution and the flow measured during test OPA7 are shown in Figure 35. When the injection pressure increased to 12 MPa under a confining pressure of 15 MPa there was a sudden increase in flow that was probably due to the piercing of the neoprene membrane. Upon dismantling it was observed that water had entered both the sample and the gas deposit connected to the top of the sample. For this reason the final water content of the sample was higher than the initial. The permeabilities computed until that moment are plotted in Figure 36, where the unexpected decrease in permeability with the decrease in effective pressure (increase in injection pressure) can be observed. As it has been explained above, this is becuase the small flow increase recorded every time the injection pressure increased, was not enough to result in a permeability increase as computed with Equation 1, in which the injection pressure has also a contribution. The permeabilities computed during the phase in which the injection pressure was 7 MPa and the confining pressure increased from 8 to 15 MPa decreased slightly from $1.3 \cdot 10^{-21}$ to $1.0 \cdot 10^{-21}$ $m^2$.

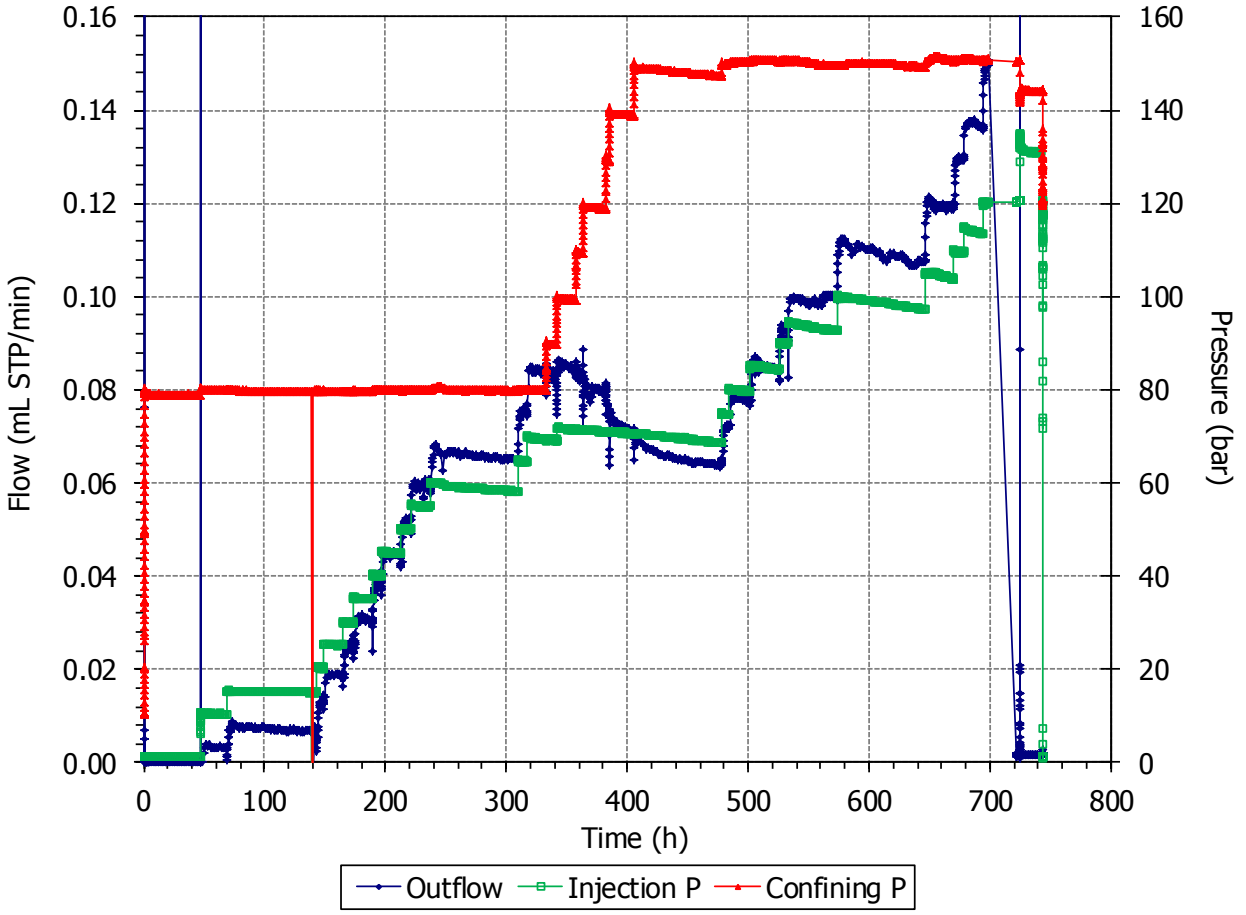


**Figure 35: Evolution of injection and confining pressure and outflow in test OPA7 (high-pressure line, cell 2)**

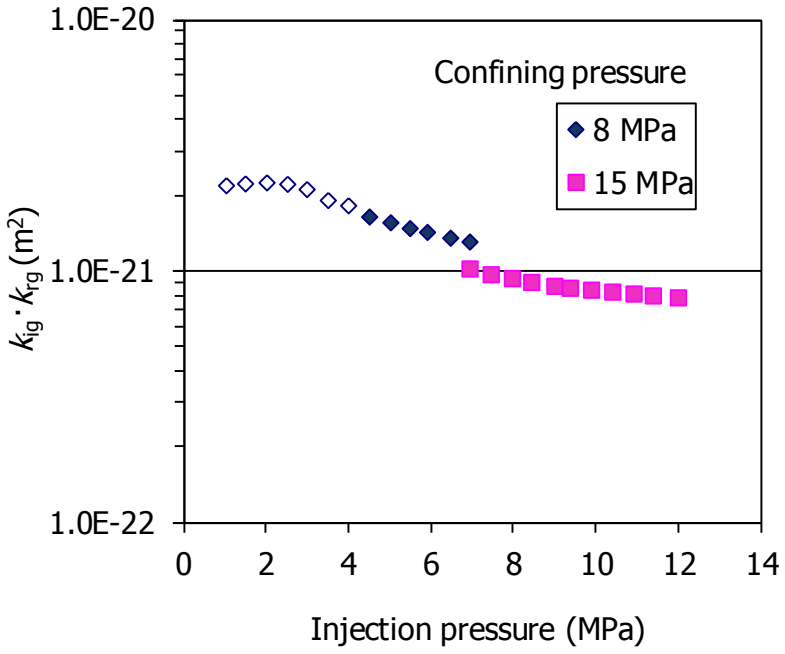


**Figure 36: Change of gas permeability with the increase in injection pressure for confining pressures 8 and 15 MPa and atmospheric backpressure in test OPA7 (the empty symbols are tentative values)**

## 4.8 TEST OPA8

The procedure described in section 3.2 and the stress path represented in Figure 11 were followed in test OPA8. The specimen was mounted in cell type 2 sandwiched between filter paper, porous stones and perforated PVC cylinders on top and bottom (Figure 37). The sample had an open stratification plane in its middle part.

**Figure 37: Initial appearance of sample OPA8 sandwiched between filter paper, porous stone and PVC cylinder on top and bottom**

The cell was pressurised to 8 MPa in the low-pressure line and the injection pressure was initially set at 1.5 MPa and increased in 0.5-MPa steps every 24 h. Once the injection pressure reached 7 MPa, the confining pressure was increased in 1-MPa steps up to 15 MPa, and then the injection pressure was increased to 13.5 MPa. At time 843 h, when the injection pressure was 8 MPa, a sudden increase in flow occurred. A similar behaviour was observed in test OPA6 and was attributed to the stretching of the sample ensemble.

The cell was changed to the high-pressure line and the confining pressure was again increased in 1-MPa steps up to 22 MPa, progressively increasing also the injection pressure up to 17.5 MPa. In the high-pressure line a different pressure regulator had to be used, for which reason the cell valves were closed and opened again once the pressures had been recovered. The outflow measured in the high-pressure line was considerably lower than that measured previously in the low-pressure line. The pressure evolution during the test along with the outflow measured is shown in Figure 38.

Both in the low and in the high-pressure lines the outflows were below the turndown point of the flowmeters, hence the measurements were not significant and no reliable permeability values could be computed. It can be considered that no measureable flow took place during the test.

For a confining pressure of 22 MPa and an injection pressure of 17.5 MPa the neoprene jacket was pierced and the water in the cell entered the gas injection pressure system. The test had to be terminated and upon dismantling the water content of the sample was determined in three different levels naturally split along the stratification planes (Figure 39). The sample was slightly drier in the upper part, where the gas was injected from, but the average final water content was similar to the initial one. According to the final dimensions, the sample seemed to have suffered expansion.

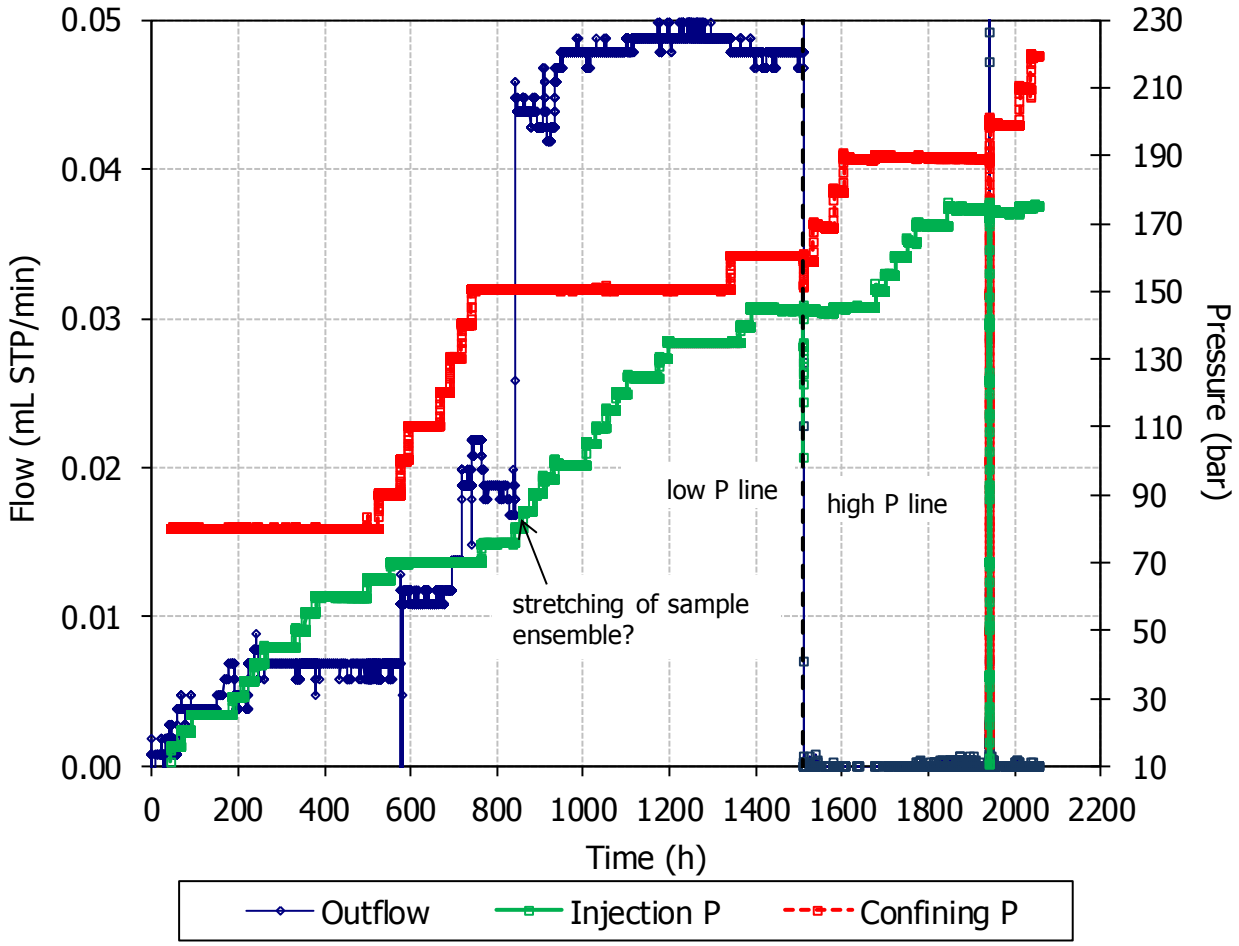


**Figure 38: Evolution of injection and confining pressure and outflow in test OPA8**

**Figure 39: Final appearance of sample OPA8, naturally split in three levels used to determine water content**

## 4.9 TEST OPA9

The procedure described in section 3.2 and the stress path represented in Figure 11 were followed in test OPA9. The sample was prepared as the previous ones, wrapped in paraffin foil, duct tape and a neoprene jacket and mounted in the high-pressure line. It was mounted in cell

type 2, with the cell modified to avoid the vertical displacements as it had been modified in test OPA4 (Figure 26).

The pressure evolution during the test is shown in Figure 40, in which the flow measured is also plotted. In most of the pressure steps, and particularly when the injection pressure was high, flow occurred, for which reason the injection pressure did not keep constant during the steps, since the pressurised gas deposit progressively emptied. This in turn made flow decrease over time in each step, because of the decrease in hydraulic gradient. The maximum confining pressure reached was 20 MPa and the maximum injection pressure was 13 MPa. This was the last step and in the course of it the injection pressure was allowed to evolve for 23 days according to the flow, i.e. without correcting its decrease.

In this test the flow measured was high enough to be considered reliable, because it was in the measurement range of the flowmeters, and the permeability computed from it is plotted in Figure 41 and Figure 42. It clearly decreased with the increase in confining pressure, but the effect of injection pressure was not so clear.

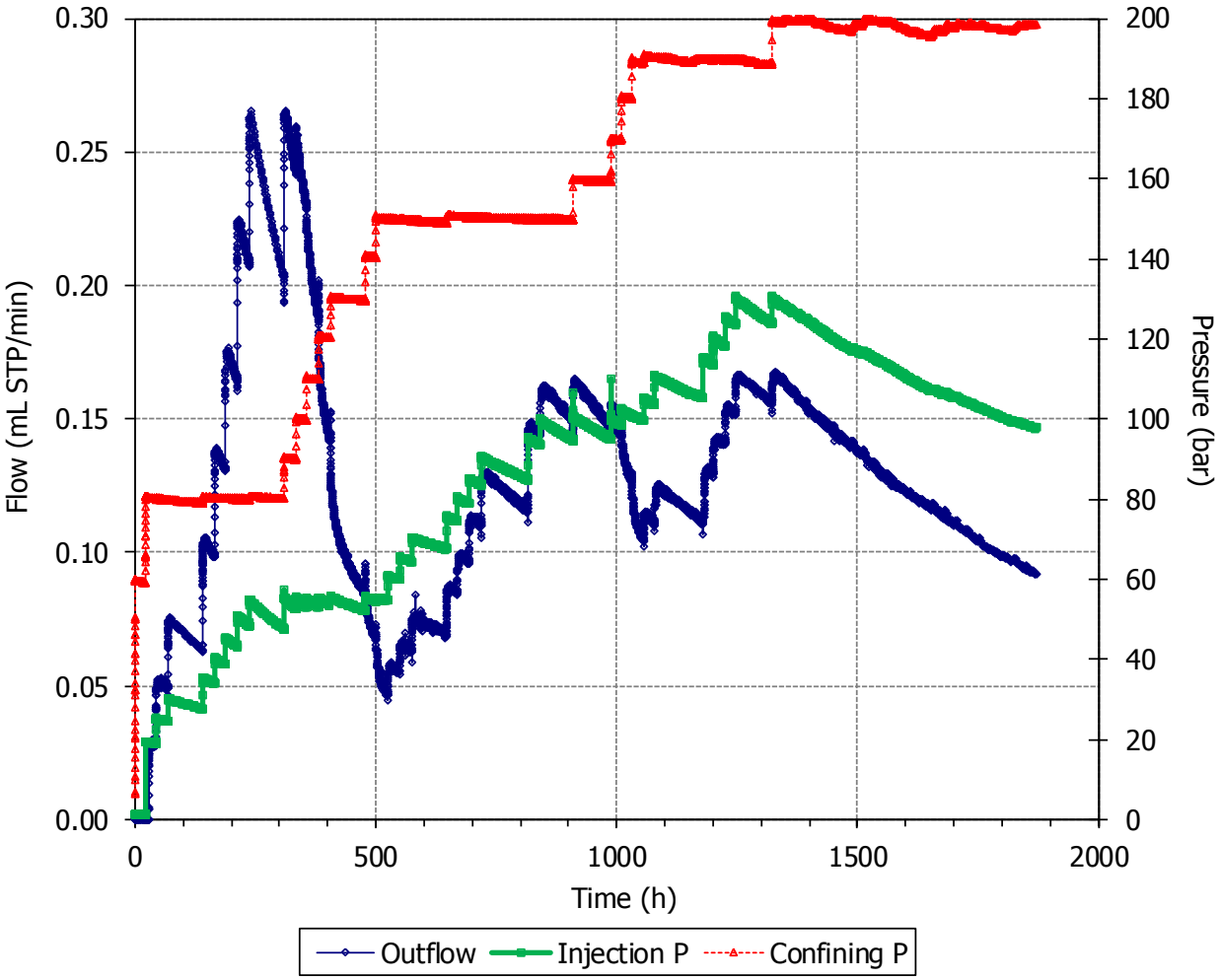


**Figure 40: Evolution of injection and confining pressure and outflow in test OPA9 (high P line)**

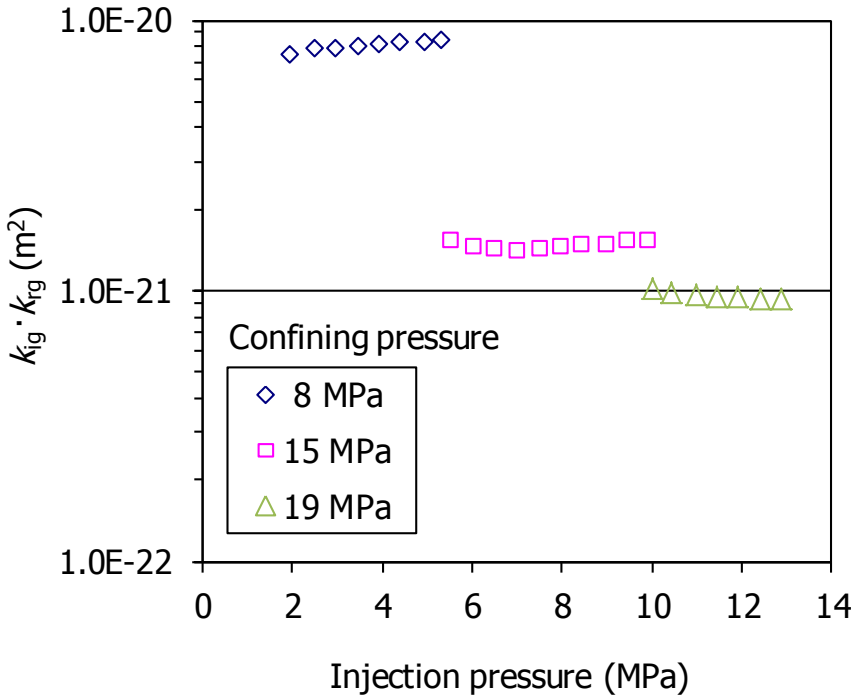


**Figure 41: Change of gas permeability with the increase in injection pressure for different confining pressures and atmospheric backpressure in test OPA9**

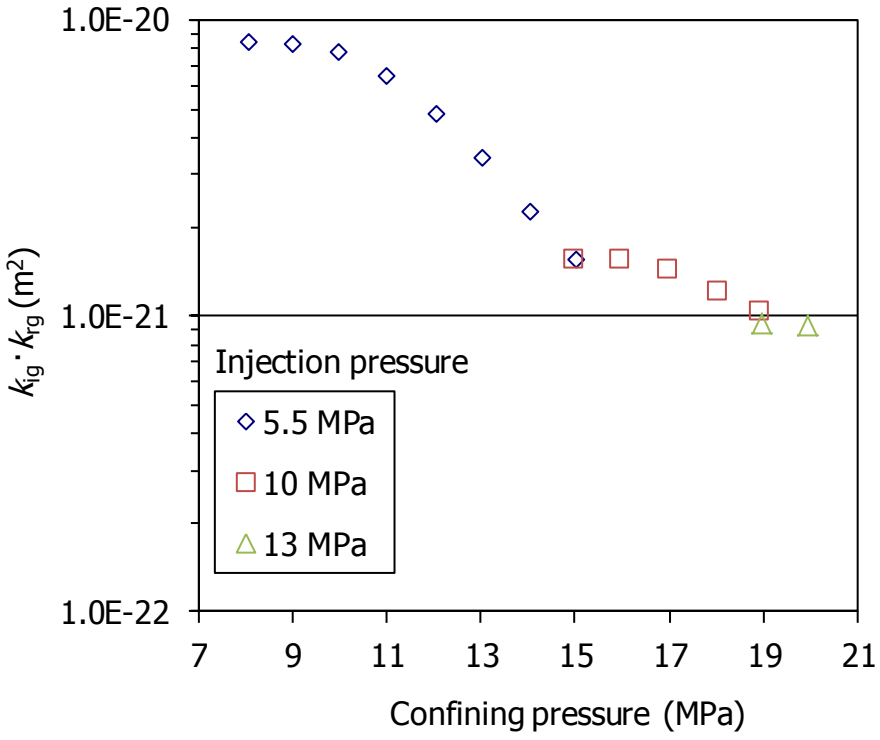


**Figure 42: Change of gas permeability with the increase in confining pressure for different injection pressures and atmospheric backpressure in test OPA9**

The sample was finally dismounted (Figure 43) and cut in three levels that were used to determine dry density and water content and pore size distribution by mercury intrusion porosimetry (MIP). Other fragments of each level were observed under a NIKON SMZ 1500

stereomicroscope. Some of them presented fissures (Figure 44), but their continuity along the core could not be verified. They could have acted as gas pathways or gas reservoirs during gas injection.

**Figure 43: Final appearance of sample OPA9**

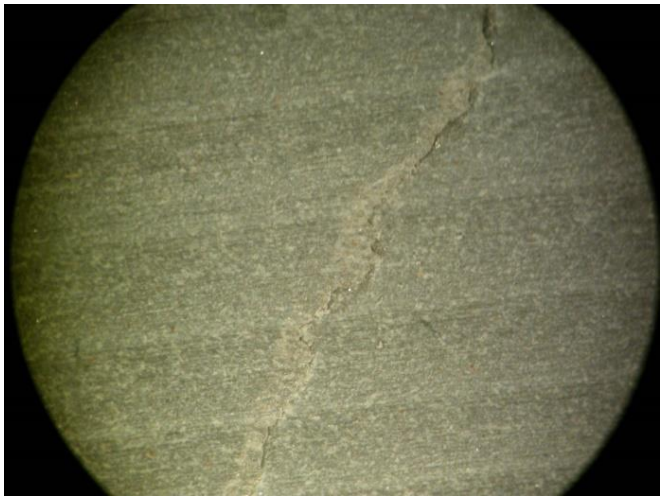

**Figure 44: Final appearance of sample OPA9 under the stereomicroscope (magnification 112.5)**

During the test the sample dried from water content 3.9 to 3.5% and it consolidated from a dry density of 2.36 to 2.39 g/cm$^3$. The pore size distribution (Figure 45) after testing was not very different to that of untested samples taken from borehole BHG-D1 presented in Villar & Romero (2012), which is also plotted in the Figure. Most of the pore sizes were comprised in the range 2-50 nm, *i.e*. in the mesopore range, with a dominant pore size mode between 8 and 15 nm, which would correspond to air entry values calculated from the Laplace's equation between 19 and 36 MPa. Only the uppermost sample, which was the one through which gas was injected, presented a higher percentage of macropores (33%) and these with a larger pore size mode.

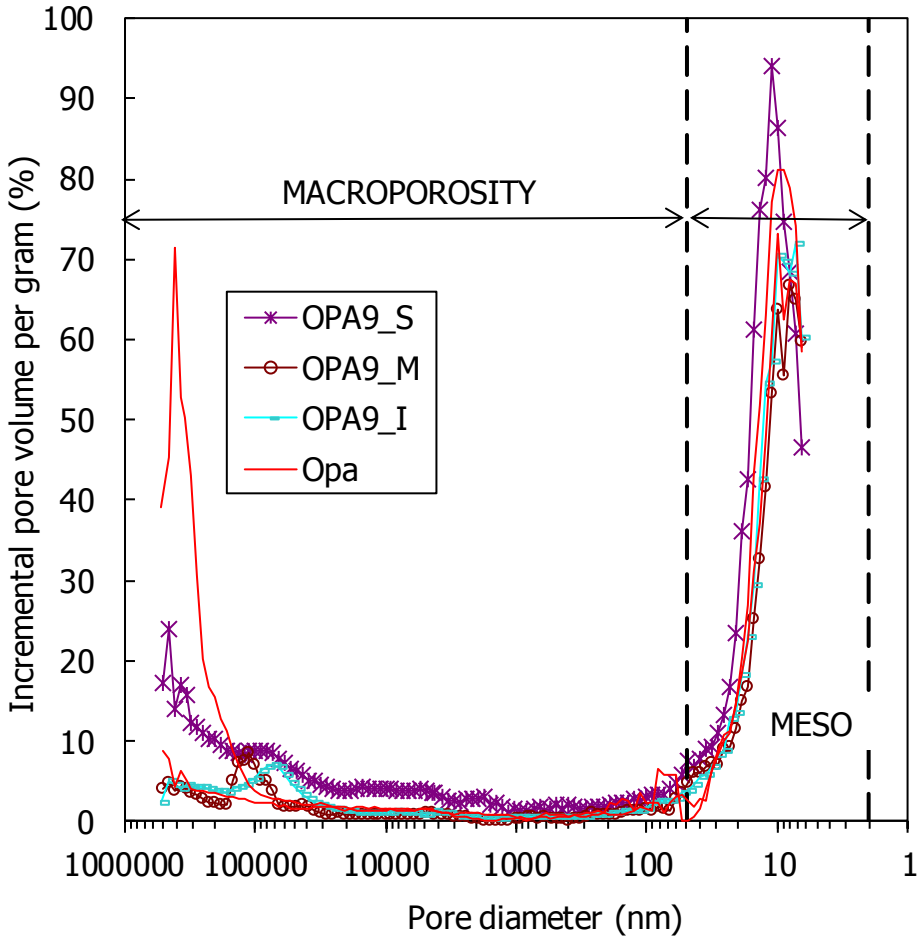


**Figure 45: Final pore size distribution obtained by MIP at three levels along sample OPA9 (s: upper, m: medium, i: lower) and for two untested Opalinus clay samples from borehole BHG-D1 (taken from Villar & Romero (2012))**

# 5 Summary and discussion of results

Nine gas permeability tests were performed in triaxial cells with Opalinus clay samples obtained by drilling from the BDR-1 core in the sense perpendicular to bedding. The average dry density of the samples was 2.31±0.04 g/cm$^3$ and water content of 4.5±1.8% ($S_r$=69±22%). The samples were not saturated prior to or during gas testing. All the tests started with a confining pressure of 8 MPa, which is slightly higher than the maximum *in situ* stress (Corkum & Martin 2007). The injection pressure was slowly increased until a value of 7 MPa (in 0.5-MPa steps applied every 24 h). Then the confining pressure was increased to 15 MPa and the injection pressure to 14 MPa (except in tests OPA2 and OPA5). Later, the pressures were increased in some tests up to values of 19 MPa for the confining pressure and 18 MPa for the injection pressure (the maximum allowed by the setup).

In most of the tests no correctly measurable outflow was detected, because the values were below the turndown value (accurate detection limit) of the flowmeters used. This would mean either that the flow was too low to be detected by the equipment used or that no flow took place because the pressures applied were below the air breakthrough value. In some instances, even if the flow was below the turndown value of the flowmeter, values higher than 0 were recorded, because the flow values measured were in fact average values obtained from around 1000 thousand data (a time-integrated value of instantaneous flow), most of which could be

zero or below their turndown value but others would be occasionally higher. This is probably an indication of turbulent flow. In this sense, the flows recorded could be at least representative of qualitative trends, even if they are not valid to compute correct permeabilities. This is particularly so in those cases in which the measurement of small flow was accompanied by pressure decreases in the upward deposit.

In those cases in which flow occurred, gas permeability ($k_{ig}{\cdot}k_{rg}$, *i.e*. intrinsic gas permeability times relative gas permeability) could be computed and the values shown in Figure 46 were obtained. The values were in the range from $8{\cdot}10^{-21}$ to $9{\cdot}10^{-22}$ $m^2$ (average $k_g$ of $2{\cdot}10^{-15}$ m/s) and tended to slightly decrease with the confining and injection pressure increase. Table V summarises the results obtained –in those cases in which the measurements could be considered representative– in terms of flow and average permeability computed from it for each confining pressure. The range of injection pressures ($P_{up}$) applied during the measurements is indicated in brackets. These average permeability values for each confining pressure have been plotted in Figure 47 as a function of the initial dry density of the samples and of the confining pressure applied during the determination. The effect of density cannot be ascertained because valid values were obtained only for two different densities. Besides, only the initial and final density values are known for each sample (Table I), since there was no specimen volume control during the tests and consequently the evolution of density during them is not known. Because of the high confining and effective pressures applied, it is likely that the dry densities during the tests were higher than the initial and the final ones.

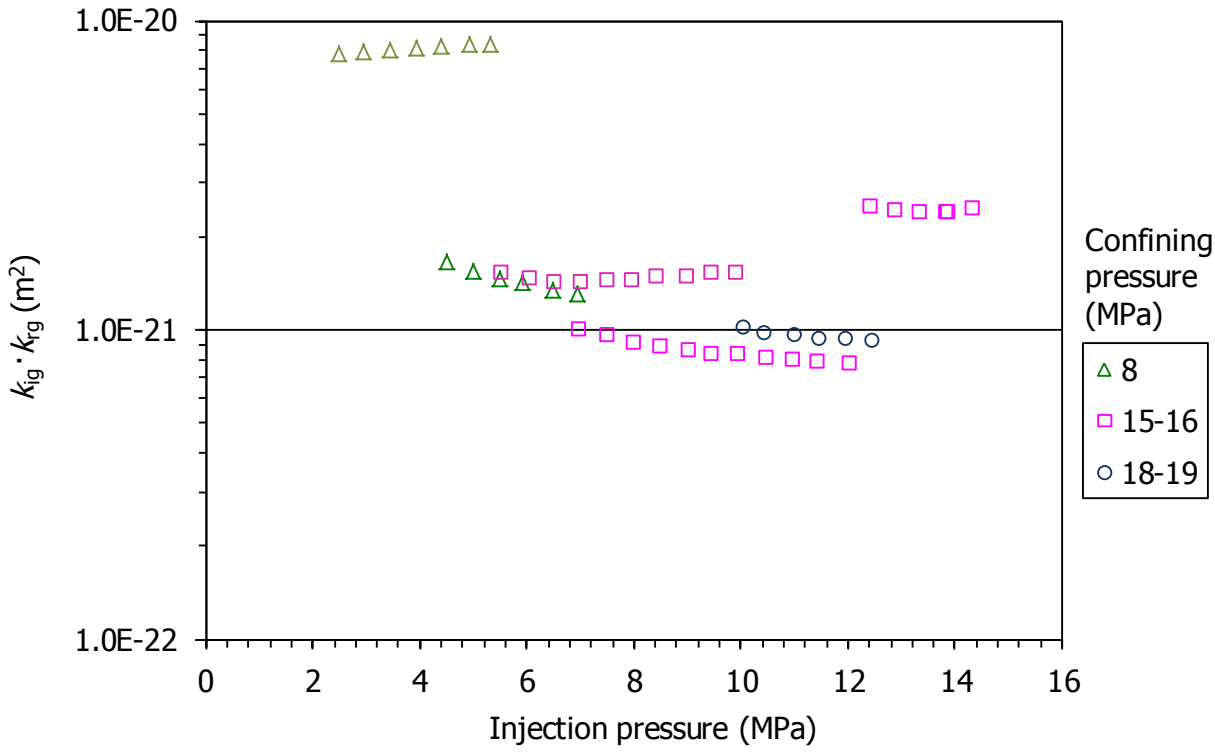


**Figure 46: Gas permeability values obtained in samples of Opalinus clay of borehole BDR-1**

**Table V: Summary of results of the gas permeability tests**

| Test reference | Confining pressure (MPa) | | | | | |
|---|---|---|---|---|---|---|
| | 8 | | 15-16 | | 18-19 | |
| | Flow (mL/min) | $k_i \cdot k_r$ ($m^2$) | Flow (mL/min) | $k_i \cdot k_r$ ($m^2$) | Flow (mL/min) | $k_i \cdot k_r$ ($m^2$) |
| OPA1 | no flow ($P_{up}$ 0.5-7 MPa) | | no flow ($P_{up}$ 7-15 MPa) | | | |
| OPA2 | no flow ($P_{up}$ 0.5-7 MPa) | | | | | |
| OPA3 | no flow ($P_{up}$ 0.5-7 MPa) | | no flow ($P_{up}$ 7-14 MPa) | | no flow ($P_{up}$ 14-18 MPa) | |
| OPA4 | no flow ($P_{up}$ 0.5-7 MPa) | | no flow ($P_{up}$ 7-14 MPa) | | no flow ($P_{up}$ 15-18 MPa) | |
| OPA4-sat | no flow ($P_{up}$ 1-6.5 MPa) | | no flow ($P_{up}$ 7 MPa) | | | |
| OPA4-sat2 | no flow ($P_{up}$ 3-6 MPa) | | no flow ($P_{up}$ 7.5-11.5 MPa) | | | |
| OPA5 | no flow ($P_{up}$ 0.5-5 MPa) | | | | | |
| OPA6 | no flow ($P_{up}$ 0.5-7 MPa) | | 0.63 ($P_{up}$ 12-14 MPa) | $2.5 \cdot 10^{-21}$ | | |
| OPA7 | 0.063 ($P_{up}$ 4.5-7 MPa) | $1.5 \cdot 10^{-21}$ | 0.103 ($P_{up}$ 7-12 MPa) | $8.7 \cdot 10^{-22}$ | | |
| OPA8 | no flow ($P_{up}$ 1-6.5 MPa) | | no flow ($P_{up}$ 7-14.5 MPa) | | no flow ($P_{up}$ 14.5-17.5 MPa) | |
| OPA9 | 0.142 ($P_{up}$ 2-5 MPa) | $8.2 \cdot 10^{-21}$ | 0.104 ($P_{up}$ 5.5-10 MPa) | $1.5 \cdot 10^{-21}$ | 0.134 ($P_{up}$ 10-13 MPa) | $9.9 \cdot 10^{-22}$ |

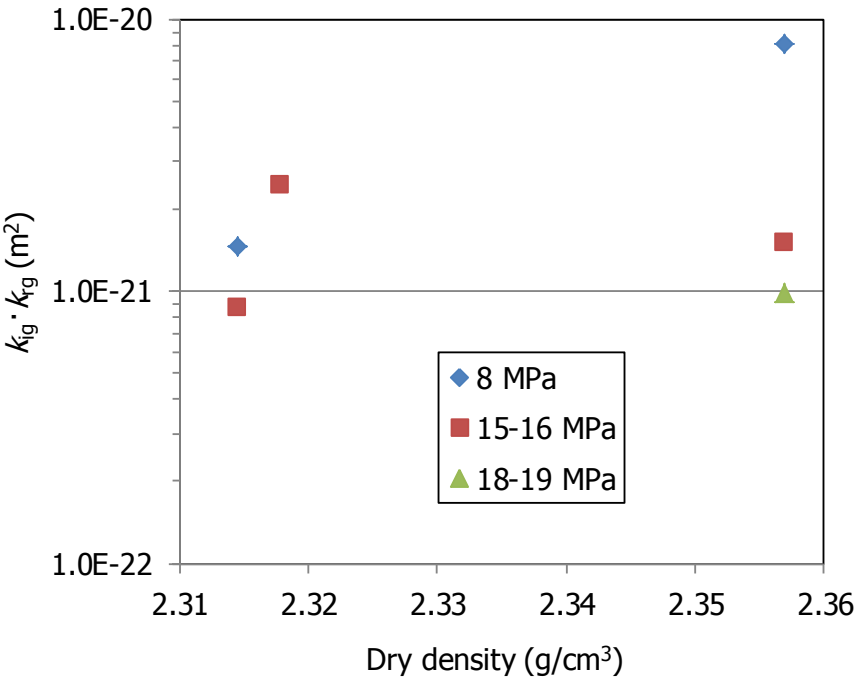


**Figure 47: Gas permeability measured for different confining pressures as a function of the initial dry density of the Opalinus clay samples of borehole BDR-1 (the dry density during the tests was probably higher)**

Since all the specimens tested came from the same borehole, had similar initial dry densities and were submitted to similar gas pressure paths, it is remarkable that flow was measured only in a few cases. The particularities of each of these are given below:

- In test OPA6 a sudden increase in flow took place for a confining pressure of 15 MPa and injection pressure of 12 MPa. A similar behaviour was observed in test OPA7 and OPA8. It is considered that this could be because of a change in the experimental setup conditions (stretching of the sample ensemble).
- In test OPA9 the cell had been modified to avoid stretching of the sample. The same modification was used in the test performed with sample OPA4 after its saturation.

The possible effect of the size of the specimens on flow has also been checked. Neither when only the significant flows are considered nor when all the measurements are taken into account is it possible to clearly relate flow and height of the sample (Figure 48).

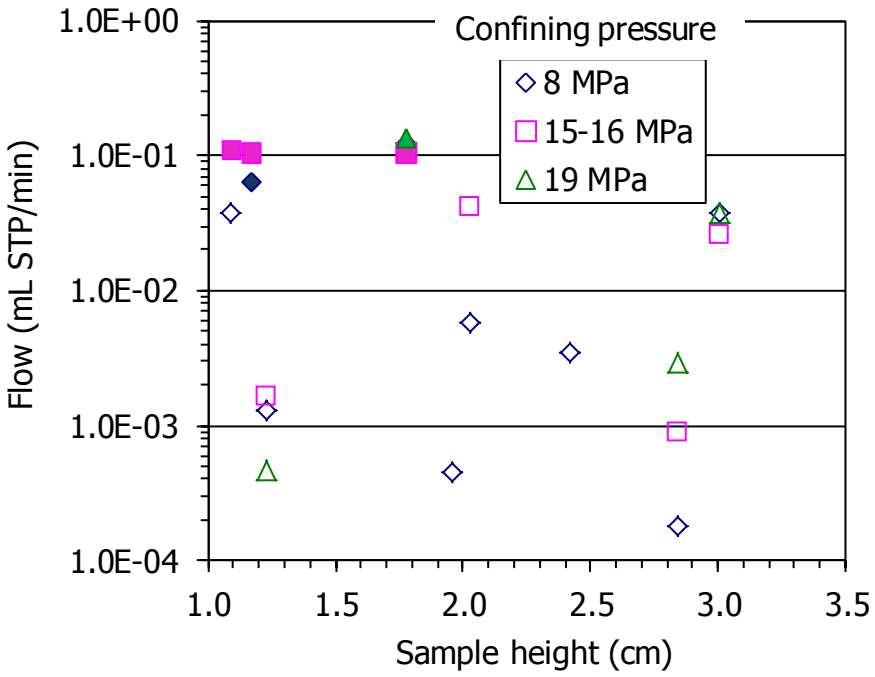


**Figure 48: Average flows measured for each confining pressure applied during the tests (various injection pressures) as a function of the sample height (tentative flow values, except filled symbols)**

Except for some experimental artefacts, such as the proper restraining of the sample (cell modification) or the temperature, it is concluded that the natural variability of the rock and the existence of features such as calcite veins or cracks that could act as preferential pathways are the responsible of the different behaviour of the samples. But, with the devices available, it was not possible to measure steady flow in most cases, which indicates that the flow was too low to be measured (maybe because it was turbulent) or that the gas breakthrough pressure in the sense perpendicular to bedding was higher than 18 MPa, which was the maximum injection pressure applied. In fact, this value is below the air entry value deduced from mercury intrusion porosimetry, which was between 19 and 36 MPa in the specimen OPA9 analysed at the end of the test and of 28 MPa in an Opalinus clay sample taken from core BHG-D1 (Villar & Romero 2012). The capillary strength parameter ($P_0$) of the van Genuchten expression fitted to results of the water retention curve of samples from boreholes BHG-D1 and BHT-1 was between 6 and

34 MPa (Villar & Romero 2012). This parameter is sometimes interpreted as representing the capillary pressure at which a continuous gas path is established. Hence, it seems that the maximum injection pressure applied in the tests presented in this report was slightly below the air entry value of the material, which could explain why flow was measured in a few instances.

It is remarkable that the samples tested were not fully saturated at the beginning of the tests, although the degree of saturation during the tests was probably higher than the initial one, because of the increase in density caused by confinement. In test OPA4 the sample was saturated after gas testing and afterwards, a gas injection test was carried out again. Although no reliable flow was measured before or after saturation, the tentative flow values measured were considerably lower after saturation.

In the air-injection tests in the sense normal to bedding performed by Senger et al. (2014) in Opalinus clay samples coming from borehole BHA-8/1, continuous gas flow occurred at an injection pressure of 12 MPa under an isotropic confining stress of 15 MPa. The $P_0$ van Genuchten parameter for the material used in these tests was 18 MPa (Romero et al. 2012), thus lower than for the material tested here. The different methodology followed by these authors to perform the gas permeability tests could also be the reason for the lower breakthrough pressure found by them. They injected air at fast volumetric-controlled rate and breakthrough took place in less than 10 min. These authors found that during gas injection, expansion and a corresponding increase in void ratio occurred associated with gas migration into the pore space of the core samples and effective stress decrease caused by the pore pressure increase. Gas continued to migrate into the expanding pores prior to the breakthrough response, which suggests that preferential gas paths were developed at increasing injection pressures, resulting in higher gas mobility and a corresponding rapid pressure recovery following gas breakthrough.

The hydraulic conductivity was measured in the direction perpendicular to bedding in two samples (OPA3 and OPA4) after the gas injection tests. For that, the samples were previously saturated, and then a hydraulic gradient was imposed under a confining stress of 1.5 MPa. The two samples had different initial dry densities and unexpectedly the higher density sample (OPA3) showed a permeability an order of magnitude higher. Although the effective stress was lower in the test performed with sample OPA3, (0.6 *vs*. 0.8 MPa) this is not considered to justify the different permeabilities, since both samples had been consolidated to much higher effective stresses during the preceding gas injection tests. Besides, despite the fact that the OPA4 sample had lower dry density than the OPA3 sample, the hydraulic gradient needed to observe flow in test OPA4 was higher than for test OPA3. Taking into account also that because of experimental problems the outflow measurement in test OPA3 lasted just 6 days, it is considered that the values obtained in this test were not reliable. Consequently, the hydraulic conductivity value in the sense normal to bedding obtained under effective stress conditions of 0.8 MPa (void ratio 0.24) would be $2.7 \cdot 10^{-14}$ m/s (corresponding to an intrinsic permeability of $2.7 \cdot 10^{-21}$ m$^2$).

Romero et al. (2012) measured in the laboratory for similar void ratios (0.20-0.24) water permeabilities an order of magnitude higher. These samples came from a different borehole (BHA-8/1) and the values measured in the sense orthogonal to bedding ranged between 1 and $3 \cdot 10^{-13}$ m/s for total stresses between 2 and 10 MPa, i.e. higher than the effective stresses applied in the tests presented here. The modelling of these results gave a value of $4.3 \cdot 10^{-20}$ m$^2$ (Senger et al. 2014). The hydraulic conductivity for the sound shaly facies as determined *in situ* (Marschall et al. 2004) is also lower than the value determined in this work.

# 6 Conclusions

Nine gas permeability tests were performed in triaxial cells with Opalinus clay samples of the shaly facies obtained by drilling from the BDR-1 core in the sense perpendicular to bedding. The average dry density of the samples was 2.31±0.04 g/cm$^3$ and water content of 4.5±1.8% ($S_r$=69±22%). The samples were not saturated prior to or during the gas testing. The confining pressures applied in these tests were higher than the maximum *in situ* stress, and the tests were performed by slowly increasing the injection pressure whereas backpressure was kept atmospheric and the outflow was measured. There was no sample volume control during the tests, but the degrees of saturation of the samples were below 100% at the beginning and end of the tests.

The gas injection tests reported showed that the breakthrough pressure in the sense perpendicular to bedding was higher than 18 MPa (effective pressure of 11.5 MPa), although in a few instances flow occurred. When this happened, the gas permeability measured ($k_{ig}$·$k_{rg}$) was in the range from 8·10$^{-21}$ to 4·10$^{-23}$ m$^2$ (average $k_g$ of 1.8·10$^{-15}$ m/s), decreasing very slightly with confining pressure. This would mean that macroscopic fracture formation (fracing, dependent on the stress state of the material) could be the mechanism for the gas flow observed, whereas in order to have 2-phase flow (without significant deformation of the pore space) much lower degrees of saturation or higher injection pressures would be needed.

The air entry value deduced from mercury intrusion porosimetry tests for this material was between 19 and 36 MPa, and this is coherent with the fact that these tests showed that the breakthrough pressure was higher than 18 MPa. Surprisingly this value is higher than the breakthrough pressure found for saturated Opalinus clay by other authors, which could be due to the natural inhomogeneity of the material or to the particularities of the experimental procedure.

The hydraulic conductivity in the sense normal to bedding obtained under effective stress conditions of 0.8 MPa (void ratio 0.24) would be 2.7·10$^{-14}$ m/s (corresponding to an intrinsic permeability of 2.7·10$^{-21}$ m$^2$).

# Acknowledgements

The research leading to these results received funding from the European Atomic Energy Community's Seventh Framework Programme (FP7/2007-2011) under Grant Agreement n$^o$230357, the FORGE project. Vanesa Gutiérrez-Rodrigo had a grant for research personnel training from CIEMAT. Part of the laboratory work was performed by Ramón Campos and Juan Aroz (CIEMAT) and the pore size distribution determinations were performed in the Petrophysics Laboratory of CIEMAT run by Dr. Rocío Campos. The Opalinus core used in this research was provided by Nagra (Dr. Paul Marschall).

# References

CORKUM, A.G., MARTIN, C.D. 2007. Modelling a mine-by test at the Mont Terri rock laboratory, Switzerland. *Int. J. Rock Mech. Min. Sci*. 44(6): 846-859.

MARSCHALL, P., CROISÉ, J., SCHLICKENRIEDER, L., BOISSON, J.-Y., VOGEL, P., YAMAMOTO, S. 2004. Synthesis of Hydrogeological Investigations at the Mont Terri Site (Phases 1 to 5). Heitzmann, P. ed. 2004: Mont Terri

Project- Hydrogeological Synthesis, Osmotic Flow. Reports of the Federal Office for Water and Geology, FOWG, Geology Series No. 6.

ROMERO, E., SENGER, R., MARSCHALL, P.; GÓMEZ, R. 2012. Air tests on low permeability claystone formations. Experimental results and simulations. In: Laloui, L. & Ferrari, A. (Eds.): Multiphysical Testing of Rocks and Shales. Springer Series in Geomechanics and Geoengineering, pp. 69-83. Springer, Berlin.

SCHEIDEGGER, A.E. 1974. *The physics of flow through porous media*. 3rd ed. Toronto: University of Toronto Press, 353 pp.

SENGER, R.; ROMERO, E.; FERRARI, A.; MARSCHALL, P. 2014. Characterization of gas flow through low-permeability experiments and two-phase flow analyses. In: Norris, S.; Bruno, J.; Cathelinau, M.; Delage, P.; Fairhurst, C.; Gaucher, E.C.; Höhn, E.H.; Kalinichev, A.; Lalieux, P.; Sellin, P. (eds.) Clays in Natural and Engineered Barriers for Radioactive Waste Confinement. Geological Society Special Publications 400. London, pp. 531-543.

VILLAR, M.V., ROMERO, F.J. 2012. Water retention curves of Opalinus clay. Informes Técnicos CIEMAT 1262. Octubre 2012. CIEMAT, Madrid, 33 pp.

# Appendix 1 TESTS RESULTS

GAS PERMEABILITY TEST
Reference: OPA1 Cell type: 1

| | Initial | Final | | Initial | Final | | |
|---|---|---|---|---|---|---|---|
| Mass (g) | | 65.50 | $\rho_d$ (g/cm$^3$) | | 2.29 | | |
| Height (cm) | | 3.010 | $w$ (%) | | 4.8 | | |
| Diameter (cm) | | 3.395 | $S_r$ (%) | | 72 | Dry mass (g) | 62.50 |

| Step | Time (h) | Outflow (mL/min) | Injection $P$ (MPa) | Confining $P$ (MPa) | Effective $P$ (MPa) | $k_{ig}\cdot k_{rg}$ (m$^2$) | $k_g$ (m/s) | $T$ (°C) |
|---|---|---|---|---|---|---|---|---|
| *LOW PRESSURE LINE* | | | | | | | | |
| 1 | 206 | 0.0008 | 0.51 | 8.00 | 7.68 | | | 22.6 |
| 2 | 235 | 0.0021 | 1.02 | 8.00 | 7.43 | | | 22.7 |
| 3 | 259 | 0.0051 | 1.52 | 8.00 | 7.18 | | | 22.5 |
| 4 | 327 | 0.0061 | 2.00 | 8.00 | 6.94 | | | 22.7 |
| 5 | 354 | 0.0091 | 2.52 | 8.00 | 6.68 | | | 22.9 |
| 6 | 375 | 0.0131 | 3.03 | 8.00 | 6.43 | | | 22.7 |
| 7 | 405 | 0.0165 | 3.50 | 8.00 | 6.19 | | | 22.8 |
| 8 | 496 | 0.0221 | 3.92 | 8.00 | 5.98 | | | 21.3 |
| 9 | 527 | 0.0268 | 4.48 | 8.00 | 5.70 | | | 22.4 |
| 10 | 625 | 0.0538 | 4.89 | 8.00 | 5.49 | | | 21.3 |
| 11 | 683 | 0.0668 | 5.52 | 8.00 | 5.18 | | | 21.9 |
| 12 | 718 | 0.0801 | 6.01 | 8.00 | 4.94 | | | 21.9 |
| 13 | 798 | 0.1021 | 6.48 | 8.00 | 4.70 | | | 21.3 |
| 14 | 882 | 0.1241 | 6.86 | 8.00 | 4.52 | | | 23.3 |
| 15 | 959 | 0.1088 | 6.86 | 9.00 | 5.51 | | | 21.1 |
| 16 | 1013 | 0.0975 | 7.07 | 10.00 | 6.40 | | | 21.1 |
| 17 | 1037 | 0.0791 | 7.03 | 11.00 | 7.42 | | | 21.6 |
| 18 | 1073 | 0.0555 | 7.00 | 12.00 | 8.43 | | | 22.0 |
| 19 | 1097 | 0.0405 | 6.98 | 13.00 | 9.45 | | | 22.1 |
| 20 | 1362 | 0.0231 | 6.67 | 14.00 | 10.60 | | | 21.1 |
| 21 | 1387 | 0.0181 | 6.95 | 15.00 | 11.46 | | | 20.6 |
| 22 | 1413 | 0.0178 | 7.54 | 15.00 | 11.16 | | | 22.1 |
| 23 | 1507 | 0.0161 | 7.93 | 15.00 | 10.97 | | | 21.7 |
| 24 | 1530 | 0.0178 | 8.47 | 15.00 | 10.70 | | | 22.0 |
| 25 | 1555 | 0.0188 | 9.02 | 15.00 | 10.43 | | | 22.6 |
| 26 | 1577 | 0.0241 | 9.46 | 15.00 | 10.21 | | | 22.0 |
| 27 | 1596 | 0.0235 | 10.01 | 15.00 | 9.93 | | | 22.3 |
| 28 | 1850 | 0.0105 | 10.51 | 15.00 | 9.69 | | | 22.9 |
| 29 | 1879 | 0.0115 | 11.02 | 15.00 | 9.43 | | | 22.8 |
| 30 | 1904 | 0.0135 | 11.50 | 15.00 | 9.19 | | | 22.7 |
| 31 | 1929 | 0.0171 | 11.85 | 15.00 | 9.01 | | | 22.4 |
| 32 | 1968 | 0.0221 | 12.13 | 15.00 | 8.87 | | | 22.3 |
| 33 | 2029 | 0.0288 | 12.87 | 15.00 | 8.50 | | | 21.9 |
| 34 | 2052 | 0.0405 | 13.48 | 15.00 | 8.19 | | | 22.1 |

| Step | Time (h) | Outflow (mL/min) | Injection *P* (MPa) | Confining *P* (MPa) | Effective *P* (MPa) | $k_{ig} \cdot k_{rg}$ ($m^2$) | $k_g$ (m/s) | *T* (°C) |
|---|---|---|---|---|---|---|---|---|
| 35 | 2076 | 0.0508 | 13.90 | 15.00 | 7.99 | | | 22.2 |
| 36 | 2110 | 0.0481 | 13.78 | 16.00 | 9.05 | | | 21.2 |
| 37 | 2310 | 0.0635 | 14.77 | 16.00 | 8.55 | | | 20.1 |
| *HIGH PRESSURE LINE* | | | | | | | | |
| 38 | 2411 | 0.0052 | 9.95 | 15.05 | 10.02 | | | 22.9 |
| 39 | 2441 | 0.0112 | 10.95 | 14.89 | 9.36 | | | 23.0 |
| 40 | 2476 | 0.0132 | 11.88 | 14.86 | 8.86 | | | 22.5 |
| 41 | 2524 | 0.0259 | 13.14 | 15.10 | 8.48 | | | 23.7 |
| 42 | 2548 | 0.0442 | 13.96 | 15.05 | 8.01 | | | 23.3 |
| 43 | 2567 | 0.0426 | 14.13 | 15.99 | 8.86 | | | 23.0 |
| 44 | 2612 | 0.0516 | 15.01 | 15.98 | 8.41 | | | 23.3 |
| 45 | 2680 | 0.0246 | 15.01 | 18.68 | 11.11 | | | 24.4 |
| 46 | 2698 | 0.0292 | 15.52 | 19.09 | 11.27 | | | 25.4 |
| 47 | 2735 | 0.0292 | 15.90 | 19.09 | 11.08 | | | 24.4 |
| 48 | 2750 | 0.0309 | 16.34 | 18.98 | 10.75 | | | 23.8 |
| 49 | 2780 | 0.0402 | 17.08 | 18.99 | 10.39 | | | 21.5 |
| 50 | 2814 | 0.0492 | 17.33 | 18.87 | 10.15 | | | 21.7 |
| 51 | 2881 | 0.0599 | 18.00 | 19.02 | 9.96 | | | 23.5 |

GAS PERMEABILITY TEST

Reference: OPA2 Cell type: 2

| | Initial | Final | | Initial | Final | | |
|---|---|---|---|---|---|---|---|
| Mass (g) | 52.92 | 54.76 | $\rho_d$ (g/$cm^3$) | 2.32 | 2.34 | | |
| Height (cm) | 2.420 | 2.420 | *w* (%) | 2.1 | 5.6 | | |
| Diameter (cm) | 3.430 | 3.415 | $S_r$ (%) | 34 | 98 | Dry mass (g) | 59.85 |

| Step | Time (h) | Outflow (mL/min) | Injection *P* (MPa) | Confining *P* (MPa) | Effective *P* (MPa) | $k_{ig} \cdot k_{rg}$ ($m^2$) | $k_g$ (m/s) | *T* (°C) |
|---|---|---|---|---|---|---|---|---|
| 1 | 502 | 0.0050 | 0.50 | 7.78 | 7.47 | | | 23.6 |
| 2 | 526 | 0.0050 | 1.00 | 8.01 | 7.44 | | | 23.7 |
| 3 | 547 | 0.0047 | 1.49 | 8.01 | 7.20 | | | 23.8 |
| 4 | 571 | | 2.02 | 8.01 | 6.95 | | | 29.0 |
| 5 | 644 | 0.0030 | 2.48 | 8.01 | 6.71 | | | 25.4 |
| 6 | 692 | 0.0030 | 2.98 | 8.01 | 6.46 | | | 25.2 |
| 7 | 716 | 0.0030 | 3.49 | 8.01 | 6.21 | | | 25.4 |
| 8 | 740 | 0.0030 | 3.97 | 8.00 | 5.96 | | | 25.3 |
| 9 | 811 | 0.0040 | 4.45 | 8.01 | 5.73 | | | 24.7 |
| 10 | 835 | 0.0043 | 4.97 | 8.01 | 5.46 | | | 24.6 |
| 11 | 859 | 0.0040 | 5.41 | 8.01 | 5.24 | | | 25.1 |
| 12 | 882 | 0.0040 | 5.99 | 8.01 | 4.96 | | | 25.2 |
| 13 | 907 | 0.0040 | 6.46 | 8.01 | 4.72 | | | 25.6 |
| 14 | 980 | 0.0040 | 6.99 | 8.01 | 4.45 | | | 25.4 |

GAS PERMEABILITY TEST

Reference: OPA3 Cell type: 1

| | Initial | Final | | Initial | Final | | |
|---|---|---|---|---|---|---|---|
| Mass (g) | 63.21 | 63.25 | $\rho_d$ (g/cm$^3$) | 2.29 | 2.22 | | |
| Height (cm) | 2.840 | 2.890 | $w$ (%) | 5.6 | 5.7 | | |
| Diameter (cm) | 3.420 | 3.450 | $S_r$ (%) | 84 | 69 | Dry mass (g) | 59.85 |

| Step | Time (h) | Outflow (mL/min) | Injection $P$ (MPa) | Confining $P$ (MPa) | Effective $P$ (MPa) | $k_{ig}\cdot k_{rg}$ (m$^2$) | $k_g$ (m/s) | $T$ (°C) |
|---|---|---|---|---|---|---|---|---|
| *HIGH PRESSURE LINE* | | | | | | | | |
| 1 | 36 | 0.0002 | 0.52 | 7.96 | 7.64 | | | 23.8 |
| 2 | 109 | 0.0000 | 1.05 | 7.71 | 7.13 | | | 23.7 |
| 3 | 229 | | 1.54 | 7.78 | 6.95 | | | 23.7 |
| 4 | 301 | | 1.98 | 8.03 | 6.98 | | | 23.6 |
| 5 | 348 | 0.0000 | 2.53 | 8.08 | 6.76 | | | 23.6 |
| 6 | 373 | 0.0000 | 3.03 | 8.06 | 6.48 | | | 23.8 |
| 7 | 397 | 0.0000 | 3.50 | 8.03 | 6.22 | | | 23.9 |
| 8 | 420 | 0.0001 | 4.07 | 8.17 | 6.08 | | | 28.3 |
| 9 | 444 | 0.0001 | 4.50 | 8.05 | 5.74 | | | 25.6 |
| 10 | 516 | 0.0004 | 5.00 | 7.97 | 5.41 | | | 25.3 |
| 11 | 565 | 0.0004 | 5.51 | 8.02 | 5.21 | | | 25.5 |
| 12 | 589 | 0.0004 | 6.00 | 8.02 | 4.96 | | | 25.3 |
| 13 | 661 | 0.0002 | 6.47 | 7.89 | 4.60 | | | 24.8 |
| 14 | 685 | 0.0002 | 6.96 | 8.00 | 4.46 | | | 24.7 |
| 15 | 709 | 0.0003 | 6.97 | 14.82 | 11.28 | | | 25.2 |
| 16 | 733 | 0.0003 | 7.54 | 14.87 | 11.04 | | | 25.3 |
| 17 | 757 | 0.0004 | 8.07 | 14.86 | 10.77 | | | 25.6 |
| 18 | 805 | 0.0004 | 8.55 | 14.54 | 10.21 | | | 25.5 |
| 19 | 853 | 0.0004 | 9.06 | 15.07 | 10.47 | | | 25.8 |
| 20 | 877 | 0.0005 | 9.59 | 15.08 | 10.23 | | | 25.7 |
| 21 | 901 | 0.0007 | 10.05 | 15.11 | 10.03 | | | 25.3 |
| 22 | 925 | 0.0009 | 10.50 | 15.04 | 9.73 | | | 25.6 |
| 23 | 973 | 0.0010 | 11.00 | 14.83 | 9.27 | | | 25.7 |
| 24 | 1021 | 0.0013 | 11.54 | 15.09 | 9.26 | | | 25.5 |
| 25 | 1045 | 0.0014 | 12.06 | 14.92 | 8.83 | | | 25.6 |
| 26 | 1069 | 0.0014 | 12.53 | 15.04 | 8.71 | | | 25.5 |
| 27 | 1117 | 0.0014 | 13.08 | 14.94 | 8.34 | | | 25.5 |
| 28 | 1188 | 0.0014 | 13.44 | 14.96 | 8.18 | | | 25.6 |
| 29 | 1213 | 0.0012 | 14.01 | 15.14 | 8.08 | | | 25.4 |
| 30 | 1237 | 0.0012 | 14.01 | 15.86 | 8.79 | | | 25.6 |
| 31 | 1261 | 0.0010 | 14.02 | 16.87 | 9.80 | | | 25.3 |
| 32 | 1309 | 0.0012 | 14.01 | 17.73 | 10.67 | | | 25.5 |
| 33 | 1357 | 0.0014 | 13.98 | 18.41 | 11.36 | | | 25.6 |
| 34 | 1381 | 0.0009 | 14.47 | 18.76 | 11.47 | | | 25.5 |
| 35 | 1405 | 0.0010 | 15.03 | 18.92 | 11.35 | | | 25.5 |
| 36 | 1429 | 0.0009 | 15.57 | 18.98 | 11.13 | | | 25.4 |
| 37 | 1453 | 0.0010 | 15.98 | 18.96 | 10.91 | | | 25.3 |
| 38 | 1525 | 0.0053 | 16.59 | 19.41 | 11.06 | $3.6\cdot10^{-23}$ | $2.6\cdot10^{-17}$ | 33.1 |
| 39 | 1549 | 0.0026 | 16.92 | 18.87 | 10.35 | | | 28.1 |
| 40 | 1597 | 0.0064 | 17.15 | 18.72 | 10.09 | $4.0\cdot10^{-23}$ | $2.9\cdot10^{-17}$ | 28.6 |
| 41 | 1693 | 0.0027 | 17.45 | 18.73 | 9.94 | | | 24.8 |

| Step | Time (h) | Outflow (mL/min) | Injection *P* (MPa) | Confining *P* (MPa) | Effective *P* (MPa) | $k_{ig} \cdot k_{rg}$ ($m^2$) | $k_g$ (m/s) | *T* (°C) |
|---|---|---|---|---|---|---|---|---|
| 42 | 1716 | 0.0031 | 17.94 | 18.88 | 9.85 | | | 24.6 |
| 43 | 1741 | 0.0028 | 18.22 | 18.94 | 9.77 | | | 24.7 |
| 44 | 1861 | 0.0036 | 18.27 | 18.96 | 9.76 | | | 24.9 |
| 45 | 2028 | 0.0035 | 18.25 | 18.92 | 9.73 | | | 24.6 |
| 46 | 2196 | 0.0041 | 18.19 | 19.02 | 9.87 | | | 24.0 |

GAS PERMEABILITY TEST
Reference: OPA4 Cell type: 2

| | Initial | Final | | Initial | Final | | |
|---|---|---|---|---|---|---|---|
| Mass (g) | 27.17 | 27.12 | $\rho_d$ (g/$cm^3$) | 2.21 | 2.12 | | |
| Height (cm) | 1.230 | 1.239 | *w* (%) | 7.5 | 7.3 | | |
| Diameter (cm) | 3.440 | 3.501 | $S_r$ (%) | 90 | 71 | Dry mass (g) | 25.27 |

| Step | Time (h) | Outflow (mL/min) | Injection *P* (MPa) | Confining *P* (MPa) | Effective *P* (MPa) | $k_{ig} \cdot k_{rg}$ ($m^2$) | $k_g$ (m/s) | *T* (°C) |
|---|---|---|---|---|---|---|---|---|
| *LOW PRESSURE LINE* | | | | | | | | |
| 1 | 106 | 0.0000 | 0.49 | 8.02 | 7.71 | | | 25.6 |
| 2 | 130 | 0.0000 | 1.02 | 8.01 | 7.44 | | | 25.5 |
| 3 | 154 | 0.0000 | 1.52 | 8.01 | 7.20 | | | 25.4 |
| 4 | 178 | 0.0000 | 2.11 | 8.01 | 6.90 | | | 25.4 |
| 5 | 202 | 0.0003 | 2.49 | 8.01 | 6.71 | | | 25.3 |
| 6 | 274 | 0.0000 | 3.01 | 8.03 | 6.47 | | | 33.1 |
| 7 | 298 | 0.0000 | 3.48 | 8.02 | 6.23 | | | 28.1 |
| 8 | 370 | 0.0000 | 4.05 | 8.05 | 5.96 | | | 32.5 |
| 9 | 442 | 0.0016 | 4.44 | 8.04 | 5.76 | | | 24.8 |
| 10 | 466 | 0.0019 | 5.77 | 8.04 | 5.10 | | | 24.6 |
| 11 | 490 | 0.0016 | 6.22 | 8.04 | 4.87 | | | 24.7 |
| 12 | 586 | 0.0013 | 6.49 | 8.04 | 4.74 | | | 24.8 |
| 13 | 610 | 0.0009 | 6.96 | 8.04 | 4.50 | | | 24.8 |
| 14 | 634 | 0.0009 | 6.97 | 9.05 | 5.51 | | | 25.0 |
| 15 | 658 | 0.0013 | 6.97 | 10.05 | 6.51 | | | 25.0 |
| 16 | 682 | 0.0019 | 6.96 | 11.05 | 7.51 | | | 24.7 |
| 17 | 706 | 0.0019 | 6.97 | 12.06 | 8.51 | | | 24.8 |
| 18 | 778 | 0.0013 | 6.97 | 14.07 | 10.53 | | | 24.6 |
| 19 | 801 | 0.0019 | 6.97 | 15.08 | 11.53 | | | 24.6 |
| 20 | 922 | 0.0023 | 7.45 | 15.03 | 11.25 | | | 23.9 |
| 21 | 946 | 0.0016 | 7.93 | 15.04 | 11.02 | | | 23.9 |
| 22 | 970 | 0.0026 | 8.46 | 15.04 | 10.75 | | | 23.6 |
| 23 | 994 | 0.0009 | 8.97 | 15.03 | 10.49 | | | 23.9 |
| 24 | 1018 | 0.0006 | 9.54 | 15.04 | 10.21 | | | 23.9 |
| 25 | 1090 | 0.0029 | 9.90 | 15.03 | 10.02 | | | 22.9 |
| 26 | 1113 | 0.0016 | 10.49 | 15.04 | 9.74 | | | 24.2 |
| 27 | 1138 | 0.0016 | 10.98 | 15.04 | 9.49 | | | 24.3 |
| 28 | 1162 | 0.0016 | 11.47 | 15.04 | 9.25 | | | 24.3 |
| 29 | 1186 | 0.0016 | 11.94 | 15.05 | 9.01 | | | 24.2 |
| 30 | 1258 | 0.0016 | 12.49 | 15.04 | 8.74 | | | 24.4 |

| Step | Time (h) | Outflow (mL/min) | Injection *P* (MPa) | Confining *P* (MPa) | Effective *P* (MPa) | $k_{ig}{\cdot}k_{rg}$ ($m^2$) | $k_g$ (m/s) | *T* (°C) |
|---|---|---|---|---|---|---|---|---|
| 31 | 1282 | 0.0019 | 12.98 | 15.05 | 8.50 | | | 24.3 |
| 32 | 1306 | 0.0019 | 13.44 | 15.04 | 8.26 | | | 24.2 |
| 33 | 1330 | 0.0016 | 13.95 | 15.04 | 8.00 | | | 24.2 |
| 34 | 1354 | 0.0006 | 13.99 | 16.05 | 9.00 | | | 25.0 |
| 35 | 1426 | 0.0023 | 14.43 | 16.05 | 8.77 | | | 24.3 |
| 36 | 1642 | 0.0016 | 14.90 | 16.04 | 8.53 | | | 24.7 |
| *HIGH PRESSURE LINE* | | | | | | | | |
| 37 | 1810 | 0.0004 | 14.87 | 16.25 | 8.76 | | | 24.4 |
| 38 | 1834 | 0.0002 | 14.86 | 16.87 | 9.38 | | | 24.4 |
| 39 | 1857 | 0.0009 | 14.86 | 17.90 | 10.41 | | | 21.4 |
| 40 | 1906 | 0.0005 | 14.84 | 18.83 | 11.35 | | | 21.4 |
| 41 | 1954 | 0.0009 | 15.85 | 19.02 | 11.04 | | | 21.5 |
| 42 | 1978 | 0.0004 | 16.90 | 19.02 | 10.51 | | | 21.6 |
| 43 | 2050 | 0.0003 | 17.90 | 18.98 | 9.97 | | | 21.6 |
| 44 | 2818 | 0.0002 | 18.07 | 19.00 | 9.91 | | | 23.9 |

GAS PERMEABILITY TEST

Reference: OPA5 Cell type: 2

| | Initial | Final | | Initial | Final | | |
|---|---|---|---|---|---|---|---|
| Mass (g) | 43.92 | 43.92 | $\rho_d$ (g/$cm^3$) | 2.33 | 2.33 | | |
| Height (cm) | 1.960 | 1.960 | *w* (%) | 5.8 | 5.8 | | |
| Diameter (cm) | 3.405 | 3.405 | $S_r$ (%) | 96 | 96 | Dry mass (g) | 41.50 |

| Step | Time (h) | Outflow (mL/min) | Injection *P* (MPa) | Confining *P* (MPa) | Effective *P* (MPa) | $k_{ig}{\cdot}k_{rg}$ ($m^2$) | $k_g$ (m/s) | *T* (°C) |
|---|---|---|---|---|---|---|---|---|
| *LOW PRESSURE LINE* | | | | | | | | |
| 1 | 109 | 0.0004 | 0.54 | 8.01 | 7.68 | | | 21.5 |
| 2 | 134 | 0.0004 | 0.99 | 8.01 | 7.45 | | | 21.6 |
| 3 | 158 | 0.0004 | 1.50 | 8.01 | 7.20 | | | 21.5 |
| 4 | 182 | 0.0004 | 2.01 | 8.01 | 6.95 | | | 21.6 |
| 5 | 254 | 0.0004 | 2.49 | 8.01 | 6.71 | | | 21.5 |
| 6 | 280 | 0.0004 | 3.00 | 8.01 | 6.45 | | | 21.5 |
| 7 | 303 | 0.0004 | 3.50 | 8.01 | 6.20 | | | 21.5 |
| 8 | 326 | 0.0004 | 3.99 | 8.01 | 5.95 | | | 21.6 |
| 9 | 351 | 0.0004 | 4.50 | 8.01 | 5.70 | | | 21.5 |
| 10 | 421 | 0.0004 | 4.97 | 8.01 | 5.47 | | | 21.5 |
| 11 | 446 | 0.0004 | 5.49 | 8.01 | 5.21 | | | 21.6 |

GAS PERMEABILITY TEST
Reference: OPA6 Cell type: 2

| | Initial | Final | | Initial | Final | | |
|---|---|---|---|---|---|---|---|
| Mass (g) | 24.34 | 24.11 | $\rho_d$ (g/cm$^3$) | 2.32 | 2.34 | | |
| Height (cm) | 1.090 | 1.078 | $w$ (%) | 3.3 | 2.4 | | |
| Diameter (cm) | 3.445 | 3.447 | $S_r$ (%) | 53 | 41 | Dry mass (g) | 23.55 |

| Step | Time (h) | Outflow (mL/min) | Injection $P$ (MPa) | Confining $P$ (MPa) | Effective $P$ (MPa) | $k_{ig}{\cdot}k_{rg}$ (m$^2$) | $k_g$ (m/s) | $T$ (°C) |
|---|---|---|---|---|---|---|---|---|
| *LOW PRESSURE LINE* | | | | | | | | |
| 1 | 46 | 0.004 | 0.50 | 8.00 | 7.69 | | | 21.3 |
| 2 | 103 | 0.007 | 1.00 | 8.00 | 7.45 | | | 21.3 |
| 3 | 141 | 0.012 | 1.50 | 8.01 | 7.19 | | | 21.4 |
| 4 | 151 | 0.016 | 2.00 | 8.00 | 6.94 | | | 21.3 |
| 5 | 165 | 0.022 | 2.50 | 8.01 | 6.70 | | | 21.2 |
| 6 | 175 | 0.026 | 3.00 | 8.01 | 6.45 | | | 21.3 |
| 7 | 191 | 0.031 | 3.48 | 8.00 | 6.21 | | | 21.7 |
| 8 | 199 | 0.036 | 4.00 | 8.01 | 5.95 | | | 21.7 |
| 9 | 215 | 0.043 | 4.47 | 8.00 | 5.71 | | | 21.7 |
| 10 | 224 | 0.049 | 4.98 | 8.00 | 5.46 | | | 21.8 |
| 11 | 295 | 0.055 | 5.39 | 8.01 | 5.25 | | | 21.1 |
| 12 | 311 | 0.067 | 5.97 | 7.99 | 4.95 | | | 21.2 |
| 13 | 320 | 0.075 | 6.45 | 8.00 | 4.72 | | | 21.2 |
| 14 | 335 | 0.083 | 6.95 | 8.01 | 4.47 | | | 21.3 |
| 15 | 344 | 0.082 | 6.94 | 9.01 | 5.48 | | | 21.5 |
| 16 | 354 | 0.081 | 7.00 | 10.00 | 6.44 | | | 21.4 |
| 17 | 358 | 0.081 | 7.01 | 11.02 | 7.45 | | | 21.6 |
| 18 | 368 | 0.078 | 6.98 | 12.02 | 8.46 | | | 21.5 |
| 19 | 378 | 0.077 | 6.96 | 13.02 | 9.48 | | | 21.5 |
| 20 | 383 | 0.074 | 6.97 | 14.04 | 10.50 | | | 21.6 |
| 21 | 392 | 0.072 | 6.96 | 15.04 | 11.50 | | | 21.5 |
| 22 | 415 | 0.079 | 7.42 | 15.04 | 11.27 | | | 21.8 |
| 23 | 479 | 0.085 | 7.97 | 15.04 | 10.99 | | | 21.5 |
| 24 | 487 | 0.092 | 8.44 | 15.04 | 10.76 | | | 21.4 |
| 25 | 504 | 0.099 | 8.94 | 15.04 | 10.50 | | | 21.6 |
| 26 | 511 | 0.107 | 9.45 | 15.04 | 10.26 | | | 21.6 |
| 27 | 527 | 0.114 | 9.95 | 15.04 | 10.00 | | | 21.5 |
| 28 | 536 | 0.122 | 10.46 | 15.04 | 9.75 | | | 21.7 |
| 29 | 560 | 0.130 | 10.92 | 15.03 | 9.51 | | | 21.8 |
| 30 | 608 | 0.139 | 11.25 | 15.04 | 9.35 | | | 21.1 |
| 31 | 647 | 0.155 | 11.94 | 15.05 | 9.02 | | | 20.6 |
| 32 | 656 | 0.552 | 12.38 | 15.04 | 8.79 | $2.5{\cdot}10^{-21}$ | $1.9{\cdot}10^{-15}$ | 21.3 |
| 33 | 670 | 0.580 | 12.87 | 15.04 | 8.55 | $2.5{\cdot}10^{-21}$ | $1.8{\cdot}10^{-15}$ | 21.6 |
| 34 | 680 | 0.615 | 13.32 | 15.04 | 8.31 | $2.4{\cdot}10^{-21}$ | $1.8{\cdot}10^{-15}$ | 21.7 |
| 35 | 694 | 0.658 | 13.82 | 15.04 | 8.07 | $2.4{\cdot}10^{-21}$ | $1.8{\cdot}10^{-15}$ | 21.8 |
| 36 | 704 | 0.661 | 13.83 | 16.05 | 9.07 | $2.4{\cdot}10^{-21}$ | $1.8{\cdot}10^{-15}$ | 21.7 |
| 37 | 743 | 0.730 | 14.30 | 16.05 | 8.83 | $2.5{\cdot}10^{-21}$ | $1.9{\cdot}10^{-15}$ | 20.7 |
| 38 | 810 | 421.188 | 11.27 | 16.05 | 10.25 | $2.3{\cdot}10^{-18}$ | $4.6{\cdot}10^{-12}$ | 20.3 |
| 39 | 811 | 56.585 | 8.77 | 15.04 | 10.59 | $5.2{\cdot}10^{-19}$ | $4.1{\cdot}10^{-13}$ | 20.4 |
| 40 | 813 | 17.965 | 7.26 | 15.04 | 11.35 | $2.4{\cdot}10^{-19}$ | $1.8{\cdot}10^{-13}$ | 20.8 |

| Step | Time (h) | Outflow (mL/min) | Injection $P$ (MPa) | Confining $P$ (MPa) | Effective $P$ (MPa) | $k_{ig}{\cdot}k_{rg}$ ($m^2$) | $k_g$ (m/s) | $T$ (°C) |
|---|---|---|---|---|---|---|---|---|
| 41 | 819 | 5.410 | 5.92 | 15.04 | 12.02 | $1.1{\cdot}10^{-19}$ | $8.0{\cdot}10^{-14}$ | 21.6 |
| 42 | 831 | 2.448 | 4.88 | 15.03 | 12.53 | $7.2{\cdot}10^{-20}$ | $5.4{\cdot}10^{-14}$ | 20.9 |
| 43 | 855 | 1.231 | 3.91 | 15.04 | 13.03 | $5.7{\cdot}10^{-20}$ | $4.2{\cdot}10^{-14}$ | 21.0 |
| 44 | 896 | 0.546 | 3.55 | 15.02 | 13.19 | $3.0{\cdot}10^{-20}$ | $2.2{\cdot}10^{-14}$ | 21.4 |

GAS PERMEABILITY TEST
Reference: OPA7 Cell type: 2

| | Initial | Final | | Initial | Final | | |
|---|---|---|---|---|---|---|---|
| Mass (g) | 26.02 | 26.96 | $\rho_d$ (g/cm$^3$) | 2.31 | | | |
| Height (cm) | 1.170 | | $w$ (%) | 3.1 | 6.8 | | |
| Diameter (cm) | 3.445 | | $S_r$ (%) | 49 | | Dry mass (g) | 25.24 |

| Step | Time (h) | Outflow (mL/min) | Injection $P$ (MPa) | Confining $P$ (MPa) | Effective $P$ (MPa) | $k_{ig}{\cdot}k_{rg}$ ($m^2$) | $k_g$ (m/s) | $T$ (°C) |
|---|---|---|---|---|---|---|---|---|
| *HIGH PRESSURE LINE* | | | | | | | | |
| 1 | 60 | 0.003 | 1.05 | 8.00 | 7.42 | | | 21.8 |
| 2 | 133 | 0.007 | 1.51 | 7.96 | 7.15 | | | 21.1 |
| 3 | 149 | 0.012 | 2.03 | 7.97 | 6.90 | | | 21.2 |
| 4 | 158 | 0.019 | 2.53 | 7.96 | 6.63 | | | 21.1 |
| 5 | 173 | 0.025 | 3.00 | 7.97 | 6.41 | | | 21.4 |
| 6 | 181 | 0.031 | 3.52 | 7.97 | 6.15 | | | 21.5 |
| 7 | 196 | 0.039 | 4.01 | 8.00 | 5.94 | | | 21.5 |
| 8 | 204 | 0.044 | 4.50 | 8.00 | 5.69 | $1.7{\cdot}10^{-21}$ | $1.2{\cdot}10^{-15}$ | 21.5 |
| 9 | 221 | 0.052 | 5.02 | 8.00 | 5.43 | $1.6{\cdot}10^{-21}$ | $1.2{\cdot}10^{-15}$ | 21.6 |
| 10 | 229 | 0.059 | 5.50 | 8.00 | 5.19 | $1.5{\cdot}10^{-21}$ | $1.1{\cdot}10^{-15}$ | 21.5 |
| 11 | 253 | 0.066 | 5.93 | 8.00 | 4.98 | $1.4{\cdot}10^{-21}$ | $1.1{\cdot}10^{-15}$ | 21.7 |
| 12 | 317 | 0.075 | 6.47 | 7.99 | 4.70 | $1.4{\cdot}10^{-21}$ | $1.0{\cdot}10^{-15}$ | 21.5 |
| 13 | 325 | 0.084 | 6.95 | 8.00 | 4.46 | $1.3{\cdot}10^{-21}$ | $9.8{\cdot}10^{-16}$ | 21.4 |
| 14 | 340 | 0.083 | 6.92 | 8.97 | 5.45 | $1.3{\cdot}10^{-21}$ | $9.7{\cdot}10^{-16}$ | 21.5 |
| 15 | 349 | 0.085 | 7.16 | 9.94 | 6.30 | $1.3{\cdot}10^{-21}$ | $9.3{\cdot}10^{-16}$ | 21.6 |
| 16 | 364 | 0.083 | 7.13 | 10.94 | 7.31 | $1.2{\cdot}10^{-21}$ | $9.1{\cdot}10^{-16}$ | 21.6 |
| 17 | 373 | 0.080 | 7.12 | 11.90 | 8.28 | $1.2{\cdot}10^{-21}$ | $8.8{\cdot}10^{-16}$ | 21.7 |
| 18 | 386 | 0.075 | 7.09 | 12.92 | 9.31 | $1.1{\cdot}10^{-21}$ | $8.4{\cdot}10^{-16}$ | 21.7 |
| 19 | 397 | 0.072 | 7.08 | 13.90 | 10.30 | $1.1{\cdot}10^{-21}$ | $8.0{\cdot}10^{-16}$ | 21.8 |
| 20 | 445 | 0.065 | 6.95 | 14.82 | 11.28 | $1.0{\cdot}10^{-21}$ | $7.6{\cdot}10^{-16}$ | 21.1 |
| 21 | 484 | 0.072 | 7.48 | 15.00 | 11.20 | $9.7{\cdot}10^{-22}$ | $7.2{\cdot}10^{-16}$ | 20.6 |
| 22 | 493 | 0.078 | 7.98 | 15.04 | 10.99 | $9.3{\cdot}10^{-22}$ | $6.9{\cdot}10^{-16}$ | 21.3 |
| 23 | 517 | 0.085 | 8.46 | 15.08 | 10.79 | $8.9{\cdot}10^{-22}$ | $6.7{\cdot}10^{-16}$ | 21.7 |
| 24 | 532 | 0.093 | 8.99 | 15.07 | 10.51 | $8.7{\cdot}10^{-22}$ | $6.4{\cdot}10^{-16}$ | 21.8 |
| 25 | 541 | 0.099 | 9.40 | 15.06 | 10.30 | $8.5{\cdot}10^{-22}$ | $6.3{\cdot}10^{-16}$ | 21.7 |
| 26 | 600 | 0.110 | 9.91 | 15.00 | 9.99 | $8.4{\cdot}10^{-22}$ | $6.3{\cdot}10^{-16}$ | 21.1 |
| 27 | 661 | 0.119 | 10.44 | 15.11 | 9.83 | $8.2{\cdot}10^{-22}$ | $6.2{\cdot}10^{-16}$ | 21.4 |
| 28 | 678 | 0.129 | 10.95 | 15.09 | 9.55 | $8.1{\cdot}10^{-22}$ | $6.1{\cdot}10^{-16}$ | 21.1 |
| 29 | 685 | 0.137 | 11.41 | 15.10 | 9.33 | $7.9{\cdot}10^{-22}$ | $5.9{\cdot}10^{-16}$ | 21.2 |
| 30 | 698 | 0.150 | 12.01 | 15.08 | 9.01 | $7.9{\cdot}10^{-22}$ | $5.9{\cdot}10^{-16}$ | 21.0 |

GAS PERMEABILITY TEST
Reference: OPA8 Cell type: 2

| | Initial | Final | | Initial | Final | | |
|---|---|---|---|---|---|---|---|
| Mass (g) | 56.19 | 56.19 | $\rho_d$ (g/cm$^3$) | 2.32 | 2.29 | | |
| Height (cm) | 2.030 | 2.045 | $w$ (%) | 4.7 | 4.7 | | |
| Diameter (cm) | 3.810 | 3.820 | $S_r$ (%) | 75 | 69 | Dry mass (g) | 53.67 |

| Step | Time (h) | Outflow (mL/min) | Injection $P$ (MPa) | Confining $P$ (MPa) | Effective $P$ (MPa) | $k_{ig}\cdot k_{rg}$ (m$^2$) | $k_g$ (m/s) | $T$ (°C) |
|---|---|---|---|---|---|---|---|---|
| *LOW PRESSURE LINE* | | | | | | | | |
| 1 | 36 | 0.002 | 1.1 | 8.0 | 7.4 | | | 22.4 |
| 2 | 60 | 0.004 | 1.6 | 8.0 | 7.2 | | | 23.0 |
| 3 | 84 | 0.004 | 2.0 | 8.0 | 6.9 | | | 22.7 |
| 4 | 182 | 0.007 | 2.5 | 8.0 | 6.7 | | | 21.2 |
| 5 | 204 | 0.005 | 3.0 | 8.0 | 6.4 | | | 22.6 |
| 6 | 228 | 0.007 | 3.5 | 8.0 | 6.2 | | | 21.5 |
| 7 | 252 | 0.007 | 4.0 | 8.0 | 5.9 | | | 21.4 |
| 8 | 325 | 0.007 | 4.5 | 8.0 | 5.7 | | | 21.3 |
| 9 | 348 | 0.007 | 5.0 | 8.0 | 5.5 | | | 21.4 |
| 10 | 372 | 0.007 | 5.5 | 8.0 | 5.2 | | | 21.3 |
| 11 | 494 | 0.006 | 6.0 | 8.0 | 5.0 | | | 21.4 |
| 12 | 516 | 0.007 | 6.5 | 8.0 | 4.7 | | | 21.4 |
| 13 | 540 | 0.007 | 6.5 | 9.0 | 5.7 | | | 21.2 |
| 14 | 564 | 0.007 | 7.0 | 9.0 | 5.5 | | | 21.3 |
| 15 | 588 | 0.012 | 7.0 | 10.0 | 6.5 | | | 21.2 |
| 16 | 636 | 0.012 | 7.0 | 11.0 | 7.5 | | | 21.3 |
| 17 | 684 | 0.012 | 7.0 | 12.0 | 8.5 | | | 21.3 |
| 18 | 708 | 0.014 | 7.0 | 13.0 | 9.5 | | | 21.2 |
| 19 | 732 | 0.019 | 7.0 | 14.0 | 10.5 | | | 21.3 |
| 20 | 756 | 0.022 | 7.0 | 15.0 | 11.5 | | | 21.2 |
| 21 | 805 | 0.019 | 7.6 | 15.0 | 11.2 | | | 23.8 |
| 22 | 852 | 0.044 | 8.0 | 15.1 | 11.0 | | | 25.7 |
| 23 | 876 | 0.044 | 8.5 | 15.1 | 10.7 | | | 26.4 |
| 24 | 900 | 0.043 | 9.0 | 15.0 | 10.5 | | | 26.7 |
| 25 | 924 | 0.042 | 9.5 | 15.0 | 10.2 | | | 26.3 |
| 26 | 972 | 0.048 | 9.9 | 15.0 | 10.1 | | | 21.5 |
| 27 | 1020 | 0.048 | 10.5 | 15.0 | 9.7 | | | 21.6 |
| 28 | 1044 | 0.048 | 11.0 | 15.0 | 9.5 | | | 21.3 |
| 29 | 1068 | 0.048 | 11.5 | 15.0 | 9.2 | | | 21.5 |
| 30 | 1092 | 0.048 | 12.0 | 15.0 | 9.0 | | | 21.4 |
| 31 | 1140 | 0.049 | 12.5 | 15.0 | 8.7 | | | 21.2 |
| 32 | 1188 | 0.049 | 13.0 | 15.0 | 8.5 | | | 21.5 |
| 33 | 1284 | 0.049 | 13.5 | 15.0 | 8.2 | | | 21.3 |
| 34 | 1356 | 0.048 | 13.5 | 16.0 | 9.2 | | | 21.7 |
| 35 | 1380 | 0.048 | 14.0 | 16.0 | 9.0 | | | 21.8 |
| 36 | 1404 | 0.048 | 14.5 | 16.0 | 8.7 | | | 21.8 |
| *HIGH PRESSURE LINE* | | | | | | | | |
| 37 | 1524 | 0.000 | 14.4 | 15.9 | 8.6 | | | 21.9 |
| 38 | 1547 | 0.000 | 14.4 | 16.9 | 9.7 | | | 21.8 |

| Step | Time (h) | Outflow (mL/min) | Injection *P* (MPa) | Confining *P* (MPa) | Effective *P* (MPa) | $k_{ig}{\cdot}k_{rg}$ ($m^2$) | $k_g$ (m/s) | *T* (°C) |
|---|---|---|---|---|---|---|---|---|
| 39 | 1596 | 0.000 | 14.5 | 17.9 | 10.6 | | | 21.3 |
| 40 | 1620 | 0.000 | 14.5 | 18.9 | 11.6 | | | 21.3 |
| 41 | 1692 | 0.000 | 15.0 | 19.0 | 11.4 | | | 21.5 |
| 42 | 1716 | 0.000 | 15.5 | 19.0 | 11.2 | | | 21.5 |
| 43 | 1740 | 0.000 | 16.0 | 19.0 | 10.9 | | | 21.6 |
| 44 | 1764 | 0.000 | 16.5 | 19.0 | 10.7 | | | 21.8 |
| 45 | 1788 | 0.000 | 17.0 | 19.0 | 10.4 | | | 21.8 |
| 46 | 1860 | 0.000 | 17.4 | 18.9 | 10.1 | | | 21.6 |
| 47 | 1956 | 0.000 | 17.4 | 19.9 | 11.2 | | | 21.4 |
| 48 | 2028 | 0.000 | 17.5 | 21.0 | 12.2 | | | 21.9 |
| 49 | 2052 | 0.000 | 17.5 | 21.9 | 13.1 | | | 22.1 |

GAS PERMEABILITY TEST
Reference: OPA9 Cell type: 2

| | Initial | Final | | Initial | Final | | |
|---|---|---|---|---|---|---|---|
| Mass (g) | 49.32 | 49.12 | $\rho_d$ (g/$cm^3$) | 2.36 | 2.39 | | |
| Height (cm) | 1.777 | 1.750 | *w* (%) | 3.9 | 3.5 | | |
| Diameter (cm) | 3.799 | 3.800 | $S_r$ (%) | 70 | 71 | Dry mass (g) | 47.48 |

| Step | Time (h) | Outflow (mL/min) | Injection *P* (MPa) | Confining *P* (MPa) | Effective *P* (MPa) | $k_{ig}{\cdot}k_{rg}$ ($m^2$) | $k_g$ (m/s) | *T* (°C) |
|---|---|---|---|---|---|---|---|---|
| *HIGH PRESSURE LINE* | | | | | | | | |
| 1 | 36 | 0.029 | 1.9 | 8.0 | 7.0 | | | 22.2 |
| 2 | 61 | 0.051 | 2.5 | 8.0 | 6.7 | $7.8{\cdot}10^{-21}$ | $6.5{\cdot}10^{-15}$ | 22.1 |
| 3 | 85 | 0.073 | 2.9 | 8.0 | 6.4 | $7.9{\cdot}10^{-21}$ | $6.6{\cdot}10^{-15}$ | 22.0 |
| 4 | 156 | 0.101 | 3.4 | 8.0 | 6.2 | $8.1{\cdot}10^{-21}$ | $6.8{\cdot}10^{-15}$ | 21.6 |
| 5 | 180 | 0.134 | 3.9 | 8.0 | 6.0 | $8.2{\cdot}10^{-21}$ | $6.8{\cdot}10^{-15}$ | 21.8 |
| 6 | 204 | 0.169 | 4.4 | 8.0 | 5.8 | $8.3{\cdot}10^{-21}$ | $6.9{\cdot}10^{-15}$ | 21.9 |
| 7 | 228 | 0.214 | 4.9 | 8.0 | 5.5 | $8.4{\cdot}10^{-21}$ | $7.0{\cdot}10^{-15}$ | 21.7 |
| 8 | 253 | 0.252 | 5.3 | 8.1 | 5.3 | $8.4{\cdot}10^{-21}$ | $7.0{\cdot}10^{-15}$ | 21.7 |
| 9 | 324 | 0.253 | 5.4 | 9.0 | 6.3 | $8.3{\cdot}10^{-21}$ | $6.9{\cdot}10^{-15}$ | 21.5 |
| 10 | 348 | 0.238 | 5.4 | 10.0 | 7.2 | $7.8{\cdot}10^{-21}$ | $6.5{\cdot}10^{-15}$ | 21.6 |
| 11 | 372 | 0.197 | 5.4 | 11.0 | 8.2 | $6.5{\cdot}10^{-21}$ | $5.4{\cdot}10^{-15}$ | 21.8 |
| 12 | 396 | 0.150 | 5.4 | 12.0 | 9.3 | $4.8{\cdot}10^{-21}$ | $4.0{\cdot}10^{-15}$ | 21.8 |
| 13 | 420 | 0.108 | 5.5 | 13.0 | 10.2 | $3.4{\cdot}10^{-21}$ | $2.8{\cdot}10^{-15}$ | 21.7 |
| 14 | 492 | 0.071 | 5.5 | 14.1 | 11.2 | $2.2{\cdot}10^{-21}$ | $1.9{\cdot}10^{-15}$ | 21.5 |
| 15 | 516 | 0.049 | 5.5 | 15.0 | 12.2 | $1.5{\cdot}10^{-21}$ | $1.3{\cdot}10^{-15}$ | 21.6 |
| 16 | 540 | 0.057 | 6.0 | 15.0 | 11.9 | $1.5{\cdot}10^{-21}$ | $1.2{\cdot}10^{-15}$ | 21.5 |
| 17 | 564 | 0.065 | 6.5 | 15.0 | 11.7 | $1.5{\cdot}10^{-21}$ | $1.2{\cdot}10^{-15}$ | 21.6 |
| 18 | 588 | 0.074 | 7.0 | 15.0 | 11.4 | $1.4{\cdot}10^{-21}$ | $1.2{\cdot}10^{-15}$ | 21.4 |
| 19 | 660 | 0.087 | 7.5 | 15.1 | 11.3 | $1.5{\cdot}10^{-21}$ | $1.2{\cdot}10^{-15}$ | 21.4 |
| 20 | 684 | 0.098 | 7.9 | 15.0 | 11.0 | $1.5{\cdot}10^{-21}$ | $1.2{\cdot}10^{-15}$ | 21.0 |
| 21 | 708 | 0.112 | 8.4 | 15.0 | 10.8 | $1.5{\cdot}10^{-21}$ | $1.2{\cdot}10^{-15}$ | 21.2 |
| 22 | 732 | 0.129 | 9.0 | 15.0 | 10.5 | $1.5{\cdot}10^{-21}$ | $1.3{\cdot}10^{-15}$ | 21.4 |
| 23 | 828 | 0.147 | 9.4 | 15.0 | 10.2 | $1.6{\cdot}10^{-21}$ | $1.4{\cdot}10^{-15}$ | 21.2 |

| Step | Time (h) | Outflow (mL/min) | Injection *P* (MPa) | Confining *P* (MPa) | Effective *P* (MPa) | $k_{ig} \cdot k_{rg}$ ($m^2$) | $k_g$ (m/s) | *T* (°C) |
|---|---|---|---|---|---|---|---|---|
| 24 | 852 | 0.161 | 9.9 | 15.0 | 10.0 | $1.6 \cdot 10^{-21}$ | $1.4 \cdot 10^{-15}$ | 21.2 |
| 25 | 924 | 0.162 | 9.9 | 16.0 | 10.9 | $1.5 \cdot 10^{-21}$ | $1.4 \cdot 10^{-15}$ | 21.5 |
| 26 | 996 | 0.150 | 9.9 | 17.0 | 11.9 | $1.4 \cdot 10^{-21}$ | $1.3 \cdot 10^{-15}$ | 21.1 |
| 27 | 1020 | 0.132 | 10.1 | 18.0 | 12.9 | $1.2 \cdot 10^{-21}$ | $1.1 \cdot 10^{-15}$ | 21.3 |
| 28 | 1044 | 0.109 | 10.0 | 18.9 | 13.8 | $1.0 \cdot 10^{-21}$ | $9.5 \cdot 10^{-16}$ | 21.2 |
| 29 | 1068 | 0.114 | 10.4 | 19.0 | 13.8 | $9.9 \cdot 10^{-22}$ | $9.1 \cdot 10^{-16}$ | 21.0 |
| 30 | 1092 | 0.124 | 11.0 | 19.0 | 13.5 | $9.7 \cdot 10^{-22}$ | $8.9 \cdot 10^{-16}$ | 21.5 |
| 31 | 1188 | 0.131 | 11.4 | 19.0 | 13.2 | $9.4 \cdot 10^{-22}$ | $8.7 \cdot 10^{-16}$ | 21.5 |
| 32 | 1212 | 0.142 | 11.9 | 19.0 | 12.9 | $9.4 \cdot 10^{-22}$ | $8.7 \cdot 10^{-16}$ | 21.5 |
| 33 | 1236 | 0.154 | 12.4 | 19.0 | 12.7 | $9.4 \cdot 10^{-22}$ | $8.6 \cdot 10^{-16}$ | 21.5 |
| 34 | 1260 | 0.166 | 12.9 | 19.0 | 12.4 | $9.4 \cdot 10^{-22}$ | $8.6 \cdot 10^{-16}$ | 21.5 |
| 35 | 1332 | 0.166 | 13.0 | 19.9 | 13.4 | $9.3 \cdot 10^{-22}$ | $8.6 \cdot 10^{-16}$ | 21.1 |

1135-9420